Comparing macroscopic continuum models for rarefied gas dynamics: A new test method

Yingsong Zheng

Department of Mechanical Engineering, University of Strathclyde, Glasgow G1 1XJ, UK

yingsong.zheng@strath.ac.uk, Tel: +44-141-548-4497, Fax: +44-141-552-5105

Jason M. Reese

Department of Mechanical Engineering, University of Strathclyde, Glasgow G1 1XJ, UK

jason.reese@strath.ac.uk, Tel: +44-141-548-3131, Fax: +44-141-552-5105

Henning Struchtrup[1]

Department of Mechanical Engineering, University of Victoria, Victoria V8W 3P6, Canada

struchtr@me.uvic.ca, Tel: +1-250-721-8916, Fax: +1-250-721-6051

Mathematics Subject Classification: 65Nxx, 76P05

[1] Corresponding author

Abstract

We propose a new test method for investigating which macroscopic continuum models, among the many existing models, give the best description of rarefied gas flows over a range of Knudsen numbers. The merits of our method are: no boundary conditions for the continuum models are needed, no coupled governing equations are solved, while the Knudsen layer is still considered. This distinguishes our proposed test method from other existing techniques (such as stability analysis in time and space, computations of sound speed and dispersion, and the shock wave structure problem). Our method relies on accurate, essentially noise-free, solutions of the basic microscopic kinetic equation, e.g. the Boltzmann equation or a kinetic model equation; in this paper, the BGK model and the ES-BGK model equations are considered.

Our method is applied to test whether one-dimensional stationary Couette flow is accurately described by the following macroscopic transport models: the Navier-Stokes-Fourier equations, Burnett equations, Grad's 13 moment equations, and the Regularized 13 moment equations (two types: the original, and that based on an order of magnitude approach). The gas molecular model is Maxwellian.

For Knudsen numbers in the transition-continuum regime ($Kn \leq 0.1$), we find that the two types of Regularized 13 moment equations give similar results to each other, which are better than Grad's original 13 moment equations, which, in turn, give better results than the Burnett equations. The Navier-Stokes-Fourier equations give the worst results. This is as expected, considering the presumed accuracy of these models. For cases of higher Knudsen numbers, i.e. $Kn > 0.1$, all macroscopic continuum equations tested fail to describe the flows accurately.

We also show that the above conclusions from our tests are general, and independent of the kinetic model used.

Keywords: Non-Continuum Effects, Rarefied Gas Flows, Microfluidics, Burnett Equations, Moment Equations

1. Introduction

The Boltzmann equation is the basic mathematical description of rarefied gas flows commonly encountered in aerodynamics, environmental problems, aerosol reactors, micromachines, the vacuum industry, etc. [1, 2]. Kinetic models with simplified expressions for the molecular collision term are often considered in order to reduce the mathematical complexity of the original Boltzmann equation [2-4]. Macroscopic continuum-type equations for rarefied gas flows can also be derived from the Boltzmann equation, or from other kinetic models, by a variety of means [4] including the Chapman-Enskog method [2-7], Grad's moment method [4, 5, 8], and variations and combinations of these [4, 9-22].

Consequently, many competing Macroscopic Continuum Models (MCMs) are now available in the literature. These include the Navier-Stokes-Fourier (NSF) equations and the Burnett equations from the traditional Chapman-Enskog expansion method [2-7], the Augmented Burnett equations [9], Chen & Spiegel's modified NSF and Burnett equations [10, 11], the Regularized Burnett equations [12, 13], Grad's 13 moment equations (abbreviated as Grad13 in this paper) [4, 5, 8], moment equations from some method related to maximum entropy [14, 15, 16], 13 moment equations from consistent order extended thermodynamics [17], the original Regularized 13 equations (abbreviated as R13A in this paper) [3, 4, 18, 19], and Regularized 13 equations based on an order of magnitude approach (abbreviated as R13B in this paper) [3, 4, 20, 21], NSF equations with a wall function technique [22], and others.

Evidently, it is necessary now to develop some way of assessing which MCM gives the best description of rarefied gas flows. Several test techniques are routinely used to examine the capabilities of MCMs, including the computation of shock wave structures [4, 19, 23], tests of temporal and spatial stability [4, 18, 19, 24], dispersion and damping of sound waves [4, 11,

18], thermodynamic consistency (validity of the 2nd law of thermodynamics) [12, 14-17], and description of the Knudsen layer in Couette flow [4, 25] (or its limiting case, Kramer's problem [26]).

Since boundary conditions for sets of MCMs are still in development, non-mature and inconsistent [4, 20, 25-27], existing test techniques (except the description of Couette flow and Kramer's problem) do not generally predict the flow in the Knudsen layer, even though this is a very important aspect of rarefied gas dynamics [2, 5, 28]. In [25], only the general structure of linear solutions of several MCMs applied to the Knudsen layer in Couette flow was discussed, and some coefficients still need to be determined by the unknown boundary conditions. In [26], these boundary conditions were obtained from the kinetic theory solution of Kramer's problem based on the linearized BGK model.

In this paper we present an alternative test method for assessing MCMs for rarefied gas dynamics. It allows us to incorporate the Knudsen layer without requiring boundary conditions but relies on an accurate numerical solution of the microscopic equation (e.g. the Boltzmann equation, or other kinetic model equations). This allows us to compute accurate values of macroscopic quantities (i.e. the moments of the distribution function), such as mass density ρ, temperature T, velocity u_i, pressure tensor p_{ij}, viscous stress (or pressure deviator) σ_{ij}, and heat flux q_i. In this paper we call the values of these moments from this type of computation "direct values".

In our test method, the viscous stress and the heat flux are calculated from the corresponding expressions in a MCM for a specific flow, where values of the moments in the MCM expressions are chosen to be the direct values obtained from the kinetic theory computations.

Any differences between the values of the viscous stress and heat flux calculated in this manner and their direct values is then a measure of the quality of the MCM. An MCM can be considered to be more physically realistic (at least for this test flow) than another when its calculated values of viscous stress and heat flux are closer to the direct values.

We also note that this test technique does not require a solution of the governing equations of the MCMs (coupled partial differential equations), but even so real rarefied gas flows involving the Knudsen layer are considered using the full equations, not just linear solutions as in [25, 26]. On the other hand, our method requires the solution of a kinetic equation for rarefied flows, which is numerically expensive. The spatial derivatives of moments using their direct values are required in the tests, which means a high accuracy is needed of the computations of the kinetic equations.

The most common method for simulating rarefied gas flows — Direct Simulation Monte Carlo (DSMC) [29] — could be used here, although very intensive computational effort is required to limit the amount of stochastic noise which can spoil our calculations of spatial derivatives. In this paper, we use instead a deterministic solver for the kinetic models proposed by Mieussens [30-32].

At present, the complete boundary conditions for all higher order MCMs are not known. While their importance was realized several decades ago [5, 8], the computation of the boundary conditions still is an unresolved problem [4]. It must be noted that the boundary conditions will not be the same for the various MCMs. Nevertheless, our proposed test method helps to determine which MCMs would be better than others for the description of rarefied gas flows, especially when the Knudsen layer flow is important. The benefit of this

work is that the research community do not need to develop boundary conditions for every MCM, we just need to focus on which MCM shows better results than others. If the additional boundary conditions are developed in the future, this test method becomes unnecessary and obsolete.

In this paper, we investigate the effectiveness of the NSF equations, the Burnett equations, the Grad13, the R13A and the R13B from the BGK model and the ES-BGK model [7, 32-34] with a Prandtl number Pr=2/3, for a one-dimensional steady Couette flow. We model the gas as Maxwellian molecules [1-4, and Appendix B]. A brief description of the Boltzmann equation, BGK model and ES-BGK model is given in Appendix A.

2. Macroscopic continuum models

In continuum theories of rarefied gas dynamics, the state of the gas is described by macroscopic quantities such as mass density, ρ, macroscopic flow velocity, u_i, temperature, T, which depend on position, x_i, and time, t. These quantities are moments of the particle distribution function, f, in the Boltzmann equation [1-7] and are obtained by taking velocity averages of the corresponding microscopic quantities, i.e.

$$\rho = m\int f dc_1 dc_2 dc_3 = m\int f d\mathbf{c}, \qquad \rho u_i = m\int c_i f d\mathbf{c},$$

$$\rho e = \frac{3}{2}p = \frac{3}{2}\rho RT = \frac{m}{2}\int C^2 f d\mathbf{c}, \qquad p_{ij} = p\delta_{ij} + \sigma_{ij} = m\int f C_i C_j d\mathbf{c},$$

$$\sigma_{ij} = m\int f C_{<i} C_{j>} d\mathbf{c}, \qquad q_i = \frac{m}{2}\int C^2 C_i f d\mathbf{c}, \tag{1}$$

$$\rho_{<ijk>} = m\int f C_{<i} C_j C_{k>} d\mathbf{c}, \qquad \rho_{rr<ij>} = m\int f C^2 C_{<i} C_{j>} d\mathbf{c},$$

$$\rho_{rrss} = m\int f C^4 d\mathbf{c},$$

where ρe is the internal energy density, $R = k/m$ is the gas constant, k is Boltzmann's constant, m is the mass of a molecule, c_i is the microscopic particle velocity, $C_i = c_i - u_i$ is the peculiar velocity, p is the hydrostatic pressure, p_{ij} is the pressure tensor, q_i is the heat flux , σ_{ij} is the viscous stress (and an angular bracket around indices denotes the symmetric and trace-free part of a tensor, i.e. $C_{<i}C_{j>} = C_iC_j - C^2\delta_{ij}/3$; for more details on the computation of symmetric and trace-free tensors, see [4, 21]). The third expression in Eqs. (1) gives the definition of temperature based on the ideal gas law. Higher order moments ρ_{ijk}, $\rho_{rr<ij>}$ and ρ_{rrss} appear in the 13 moment equations in Section 2.2 below.

Multiplying the Boltzmann equation successively by 1, c_i, and $c^2/2$, then integrating over particle phase velocity and utilizing the conservation laws at the microscopic level [2, 4], yields the macroscopic conservation laws for mass, momentum and energy,

$$\frac{\partial \rho}{\partial t} + \frac{\partial(\rho u_i)}{\partial x_i} = 0, \tag{2.a}$$

$$\frac{\partial \rho u_i}{\partial t} + \frac{\partial}{\partial x_j}(\rho u_i u_j + p_{ij}) = 0, \tag{2.b}$$

$$\frac{\partial}{\partial t}\left(\rho e + \frac{1}{2}\rho u_i^2\right) + \frac{\partial}{\partial x_j}\left(\rho e u_j + \frac{1}{2}\rho u^2 u_j + u_i p_{ij} + q_j\right) = 0. \tag{2.c}$$

Note that this set of equations (which is exact, without any assumption or approximation, and should be satisfied by any MCM) is not closed unless additional equations for the viscous stress, σ_{ij}, and heat flux, q_i, are given. These additional equations can be obtained from the Boltzmann equation or kinetic models through different methods that always involve some assumptions and/or approximations.

In some MCMs — such as the NSF, the Burnett equations [2-7], Augmented Burnett equations [9], and the NSF equations with a wall function technique [22] — σ_{ij} and q_i are expressed as *explicit* functions of density, velocity, temperature and their spatial derivatives, which means the constitutive relations for σ_{ij} and q_i are not governing equations of similar form to the conservation laws Eqs. (2). The set of equations in this type of MCM have only five independent variables in general three dimensional problems. We denote these MCMs as "first type" MCMs.

In other MCMs — such as Chen and Spiegel's modified NSF and Burnett equations [10, 11], the Regularized Burnett equations [12, 13], the Grad13 [5, 8], moment equations from some method related to maximum entropy [14-16], 13 moment equations from consistent order extended thermodynamics [17], the R13A [3, 4, 18, 19] and the R13B [3, 4, 20, 21] — σ_{ij} and q_i can only be expressed as *implicit* functions of density, velocity, temperature. The equations for σ_{ij} and q_i are coupled governing equations in the system, in addition to the conservation laws Eqs. (2). This means that the number of variables in these sets of equations is thirteen (or sometimes more) in general three dimensional problems. These MCMs are denoted as "second type" MCMs here.

In this paper, we consider one-dimensional steady Couette flow between two parallel plates a distance L apart, with one plate moving in the x_1 direction; the direction perpendicular to the plates is x_2. Therefore the velocities $u_2 = u_3 = 0$, and $\partial/\partial x_1 = \partial/\partial x_2 = 0$. The unknown quantities in the viscous stress and heat flux for this flow are σ_{11}, σ_{22}, σ_{12}, q_1, and q_2, while $\sigma_{33} = -(\sigma_{11} + \sigma_{22})$, $\sigma_{21} = \sigma_{12}$, $\sigma_{31} = \sigma_{13} = 0$, $\sigma_{32} = \sigma_{23} = 0$, and $q_3 = 0$.

The NSF and Burnett equations for the BGK and ES-BGK models in three dimensions are listed in Appendix B.1. The Grad13, R13A and R13B equations for the BGK and ES-BGK models in three dimensions are listed in Appendix B.2. The derivation of the corresponding governing equations for one-dimensional steady Couette flow is quite straightforward, but long and tedious and so is omitted from this paper for reasons of conciseness.

2.1. NSF and Burnett equations for the BGK and ES-BGK models

We have the following expressions for the NSF equations in one-dimensional Couette flow,

$$\sigma_{12}^{NSF} = -2\mu \frac{\partial u_{<1}}{\partial x_{2>}} = -\mu \frac{\partial u_1}{\partial x_2}, \qquad \sigma_{11}^{NSF} = \sigma_{22}^{NSF} = 0, \tag{3.a}$$

$$q_2^{NSF} = -\kappa \frac{\partial T}{\partial x_2}, \qquad q_1^{NSF} = 0. \tag{3.b}$$

Similarly, the governing Burnett equations for the ES-BGK model with Maxwellian gas molecules in one-dimensional Couette flow are,

$$\sigma_{12}^{B} = \sigma_{12}^{NSF}, \quad \sigma_{11}^{B} = \frac{\mu^2}{p^2}\Phi_{11}, \; \sigma_{22}^{B} = \frac{\mu^2}{p^2}\Phi_{22}, \tag{4.a}$$

$$q_2^{B} = q_2^{NSF}, \quad q_1^{B} = \frac{\mu^2}{p^2 \,\mathrm{Pr}}\Gamma_1, \tag{4.b}$$

where

$$\begin{aligned}\Phi_{11} = {} & \frac{2}{3}R^2T^2\frac{\partial^2\rho}{\partial x_2 \partial x_2} + \frac{2b}{3}\rho R^2 T \frac{\partial^2 T}{\partial x_2 \partial x_2} - \frac{2}{3}\frac{R^2T^2}{\rho}\frac{\partial \rho}{\partial x_2}\frac{\partial \rho}{\partial x_2} \\ & + \frac{2}{3}R^2T\frac{\partial T}{\partial x_2}\frac{\partial \rho}{\partial x_2} + \frac{4}{3}p\frac{\partial u_1}{\partial x_2}\frac{\partial u_1}{\partial x_2} - \frac{2(1-b)}{3}\rho R^2\frac{\partial T}{\partial x_2}\frac{\partial T}{\partial x_2},\end{aligned} \tag{5.a}$$

$$\begin{aligned}\Phi_{22} = {} & -\frac{4}{3}R^2T^2\frac{\partial^2\rho}{\partial x_2 \partial x_2} - \frac{4b}{3}\rho R^2 T \frac{\partial^2 T}{\partial x_2 \partial x_2} + \frac{4}{3}\frac{R^2T^2}{\rho}\frac{\partial \rho}{\partial x_2}\frac{\partial \rho}{\partial x_2} \\ & - \frac{4}{3}R^2T\frac{\partial T}{\partial x_2}\frac{\partial \rho}{\partial x_2} - \frac{2}{3}p\frac{\partial u_1}{\partial x_2}\frac{\partial u_1}{\partial x_2} + \frac{4(1-b)}{3}\rho R^2\frac{\partial T}{\partial x_2}\frac{\partial T}{\partial x_2},\end{aligned} \tag{5.b}$$

$$\Gamma_1 = pRT\frac{\partial^2 u_1}{\partial x_2 \partial x_2} - R^2T^2\frac{\partial u_1}{\partial x_2}\frac{\partial \rho}{\partial x_2} + \left(7 - \frac{7}{2}b\right)pR\frac{\partial u_1}{\partial x_2}\frac{\partial T}{\partial x_2}, \tag{5.d}$$

with $b = 1 - (1/\mathrm{Pr})$. Eqs. (4-5) simplify to the Burnett equations for the traditional BGK model when $b = 0$ [7].

From Eqs. (4-5), we can see that the expressions for shear stress, σ_{12}, and normal heat flux, q_2, are the same in both the NSF and Burnett. However, the expressions for normal stresses, σ_{11}, σ_{22}, and parallel heat flux, q_1, are different. Non-zero values of σ_{11}, σ_{22} and q_1 reflect rarefaction effects which are not described by the NSF equations.

2.2. Grad13, R13A and R13B equations for BGK and ES-BGK models

The nine basic moment equations from the general ES-BGK model for one-dimensional steady Couette flow, are the same in the Grad13, the R13A and the R13B equations, viz.

$$u_2 = 0, \tag{6.a}$$

$$\frac{\partial \sigma_{12}}{\partial x_2} = 0, \tag{6.b}$$

$$\frac{\partial p}{\partial x_2} + \frac{\partial \sigma_{22}}{\partial x_2} = 0, \tag{6.c}$$

$$\frac{\partial q_2}{\partial x_2} + \sigma_{12}\frac{\partial u_1}{\partial x_2} = 0, \tag{6.d}$$

$$-\frac{4}{15}\frac{\partial q_2}{\partial x_2} + \frac{4}{3}\sigma_{21}\frac{\partial u_1}{\partial x_2} + \frac{\partial \rho_{<112>}}{\partial x_2} = -\frac{p}{\mu}\sigma_{11}, \tag{6.e}$$

$$\frac{8}{15}\frac{\partial q_2}{\partial x_2} - \frac{2}{3}\sigma_{21}\frac{\partial u_1}{\partial x_2} + \frac{\partial \rho_{<222>}}{\partial x_2} = -\frac{p}{\mu}\sigma_{22}, \tag{6.f}$$

$$\frac{2}{5}\frac{\partial q_1}{\partial x_2} + p\frac{\partial u_1}{\partial x_2} + \sigma_{22}\frac{\partial u_1}{\partial x_2} + \frac{\partial \rho_{<122>}}{\partial x_2} = -\frac{p}{\mu}\sigma_{12}, \tag{6.g}$$

$$-\frac{5}{2}RT\frac{\partial\sigma_{12}}{\partial x_2}-\frac{\sigma_{12}}{\rho}\frac{\partial p}{\partial x_2}-\frac{\sigma_{11}}{\rho}\frac{\partial\sigma_{12}}{\partial x_2}-\frac{\sigma_{12}}{\rho}\frac{\partial\sigma_{22}}{\partial x_2}$$
$$+\frac{7}{5}q_2\frac{\partial u_1}{\partial x_2}+\frac{1}{2}\frac{\partial\rho_{rr<12>}}{\partial x_2}+\rho_{<112>}\frac{\partial u_1}{\partial x_2}=-\frac{\Pr p}{\mu}q_1\ , \tag{6.h}$$

$$-\frac{5}{2}RT\frac{\partial p}{\partial x_2}-\frac{5}{2}RT\frac{\partial\sigma_{22}}{\partial x_2}-\frac{\sigma_{22}}{\rho}\frac{\partial p}{\partial x_2}-\frac{\sigma_{21}}{\rho}\frac{\partial\sigma_{12}}{\partial x_2}-\frac{\sigma_{22}}{\rho}\frac{\partial\sigma_{22}}{\partial x_2}$$
$$+\frac{2}{5}q_1\frac{\partial u_1}{\partial x_2}+\frac{1}{2}\frac{\partial\rho_{rr<22>}}{\partial x_2}+\frac{1}{6}\frac{\partial\rho_{rrss}}{\partial x_2}+\rho_{<212>}\frac{\partial u_1}{\partial x_2}=-\frac{\Pr p}{\mu}q_2\ . \tag{6.i}$$

These equations do not form a closed set for the nine variables since they contain the higher order moments $\rho_{<112>}$, $\rho_{<122>}$, $\rho_{<222>}$, $\rho_{rr<12>}$, $\rho_{rr<22>}$ and ρ_{rrss}. The difference between the Grad13, the R13A, and the R13B equations arises from the expressions for these higher moments.

For the Grad13 equations, we have:

$$\rho^{G13}_{<112>}=\rho^{G13}_{<122>}=\rho^{G13}_{<222>}=0\,,\qquad \rho^{G13}_{rr<12>}=7RT\sigma_{12}\,, \tag{7.a}$$

$$\rho^{G13}_{rr<22>}=7RT\sigma_{22}\,,\qquad \rho^{G13}_{rrss}=15\frac{p^2}{\rho}\,. \tag{7.b}$$

For the R13A equations , we have:

$$\rho^{R13A}_{<112>}=-3\frac{\mu}{\Pr p}\left(\frac{1}{3}RT\frac{\partial\sigma_{11}}{\partial x_2}-\frac{2}{15}RT\frac{\partial\sigma_{22}}{\partial x_2}-\frac{1}{3}\frac{RT}{\rho}\sigma_{11}\frac{\partial\rho}{\partial x_2}+\frac{2}{15}\frac{RT}{\rho}\sigma_{22}\frac{\partial\rho}{\partial x_2}\right)$$
$$-3\frac{\mu}{\Pr p}\left(+\frac{16}{75}q_1\frac{\partial u_1}{\partial x_2}-\frac{1}{3}\frac{\sigma_{11}}{\rho}\frac{\partial\sigma_{22}}{\partial x_2}-\frac{8}{15}\frac{\sigma_{12}}{\rho}\frac{\partial\sigma_{12}}{\partial x_2}+\frac{2}{15}\frac{\sigma_{22}}{\rho}\frac{\partial\sigma_{22}}{\partial x_2}\right), \tag{8.a}$$

$$\rho^{R13A}_{<122>}=-3\frac{\mu}{\Pr p}\left(\frac{8}{15}RT\frac{\partial\sigma_{12}}{\partial x_2}-\frac{8}{15}\frac{RT}{\rho}\sigma_{12}\frac{\partial\rho}{\partial x_2}+\frac{16}{75}q_2\frac{\partial u_1}{\partial x_2}\right)$$
$$-3\frac{\mu}{\Pr p}\left(-\frac{1}{3}\frac{\sigma_{22}}{\rho}\frac{\partial\sigma_{12}}{\partial x_2}-\frac{8}{15}\frac{\sigma_{21}}{\rho}\frac{\partial\sigma_{22}}{\partial x_2}+\frac{2}{15}\frac{\sigma_{11}}{\rho}\frac{\partial\sigma_{12}}{\partial x_2}\right), \tag{8.b}$$

$$\rho^{R13A}_{<222>}=-3\frac{\mu}{\Pr p}\left(\frac{3}{5}RT\frac{\partial\sigma_{22}}{\partial x_2}-\frac{3}{5}\frac{RT}{\rho}\sigma_{22}\frac{\partial\rho}{\partial x_2}-\frac{4}{25}q_1\frac{\partial u_1}{\partial x_2}-\frac{3}{5}\frac{\sigma_{22}}{\rho}\frac{\partial\sigma_{22}}{\partial x_2}+\frac{2}{5}\frac{\sigma_{12}}{\rho}\frac{\partial\sigma_{12}}{\partial x_2}\right), \tag{8.c}$$

$$\rho^{R13A}_{rr<12>} = 7RT\sigma_{12} - \frac{28}{5}\frac{\mu}{\mathrm{Pr}\,p}\left(\frac{1}{2}RT\frac{\partial q_1}{\partial x_2} + \frac{1}{2}Rq_1\frac{\partial T}{\partial x_2} - \frac{1}{2}\frac{RTq_1}{\rho}\frac{\partial \rho}{\partial x_2} - \frac{1}{2}\frac{q_1}{\rho}\frac{\partial \sigma_{22}}{\partial x_2} - \frac{1}{2}\frac{q_2}{\rho}\frac{\partial \sigma_{12}}{\partial x_2}\right) - \frac{28}{5}\frac{\mu}{\mathrm{Pr}\,p}\left(\frac{5}{7}RT\left(+\frac{1}{2}\sigma_{11}\frac{\partial u_1}{\partial x_2} + \frac{1}{2}\sigma_{22}\frac{\partial u_1}{\partial x_2}\right) - \frac{5}{6}\frac{\sigma_{12}}{\rho}\frac{\partial q_2}{\partial x_2} - \frac{5}{6}\frac{\sigma_{12}}{\rho}\sigma_{12}\frac{\partial u_1}{\partial x_2}\right), \tag{8.d}$$

$$\rho^{R13A}_{rr<22>} = 7RT\sigma_{22} - \frac{28}{5}\frac{\mu}{\mathrm{Pr}\,p}\left(\frac{2}{3}RT\frac{\partial q_2}{\partial x_2} + \frac{2}{3}Rq_2\frac{\partial T}{\partial x_2} - \frac{2}{3}\frac{RTq_2}{\rho}\frac{\partial \rho}{\partial x_2} - \frac{2}{3}\frac{q_2}{\rho}\frac{\partial \sigma_{22}}{\partial x_2}\right) - \frac{28}{5}\frac{\mu}{\mathrm{Pr}\,p}\left(\frac{1}{3}\frac{q_1}{\rho}\frac{\partial \sigma_{12}}{\partial x_2} + \frac{5}{21}RT\sigma_{21}\frac{\partial u_1}{\partial x_2} - \frac{5}{6}\frac{\sigma_{22}}{\rho}\frac{\partial q_2}{\partial x_2} - \frac{5}{6}\frac{\sigma_{22}}{\rho}\sigma_{12}\frac{\partial u_1}{\partial x_2}\right), \tag{8.e}$$

$$\rho^{R13A}_{rrss} = 15\frac{p^2}{\rho} - 8\frac{\mu}{\mathrm{Pr}\,p}\left(RT\frac{\partial q_2}{\partial x_2} + \frac{5}{2}Rq_2\frac{\partial T}{\partial x_2} - \frac{RTq_2}{\rho}\frac{\partial \rho}{\partial x_2} - \frac{q_1}{\rho}\frac{\partial \sigma_{12}}{\partial x_2} - \frac{q_2}{\rho}\frac{\partial \sigma_{22}}{\partial x_2} + RT\sigma_{12}\frac{\partial u_1}{\partial x_2}\right). \tag{8.f}$$

For the R13B equations, we have:

$$\rho^{R13B}_{<112>} = -3\frac{\mu}{\mathrm{Pr}\,p}\left(\frac{1}{3}RT\frac{\partial \sigma_{11}}{\partial x_2} - \frac{2}{15}RT\frac{\partial \sigma_{22}}{\partial x_2} - \frac{1}{3}\frac{RT}{\rho}\sigma_{11}\frac{\partial \rho}{\partial x_2} + \frac{2}{15}\frac{RT}{\rho}\sigma_{22}\frac{\partial \rho}{\partial x_2} + \frac{16}{75}q_1\frac{\partial u_1}{\partial x_2}\right), \tag{9.a}$$

$$\rho^{R13B}_{<122>} = -3\frac{\mu}{\mathrm{Pr}\,p}\left(\frac{8}{15}RT\frac{\partial \sigma_{12}}{\partial x_2} - \frac{8}{15}\frac{RT}{\rho}\sigma_{12}\frac{\partial \rho}{\partial x_2} + \frac{16}{75}q_2\frac{\partial u_1}{\partial x_2}\right), \tag{9.b}$$

$$\rho^{R13B}_{<222>} = -3\frac{\mu}{\mathrm{Pr}\,p}\left(\frac{3}{5}RT\frac{\partial \sigma_{22}}{\partial x_2} - \frac{3}{5}\frac{RT}{\rho}\sigma_{22}\frac{\partial \rho}{\partial x_2} - \frac{4}{25}q_1\frac{\partial u_1}{\partial x_2}\right), \tag{9.c}$$

$$\rho^{R13B}_{rr<12>} = 7RT\sigma_{12} + \frac{2b^2}{\rho}\sigma_{12}(\sigma_{11}+\sigma_{22}) - \frac{28}{5}\frac{\mu}{\mathrm{Pr}\,p}\left(\frac{1}{2}RT\frac{\partial q_1}{\partial x_2} + \frac{1}{2}Rq_1\frac{\partial T}{\partial x_2} - \frac{1}{2}\frac{RTq_1}{\rho}\frac{\partial \rho}{\partial x_2}\right) - \frac{28}{5}\frac{\mu}{\mathrm{Pr}\,p}\left(\frac{5}{7}RT\left(+\frac{1}{2}\sigma_{11}\frac{\partial u_1}{\partial x_2} + \frac{1}{2}\sigma_{22}\frac{\partial u_1}{\partial x_2}\right)\right), \tag{9.d}$$

$$\rho^{R13B}_{rr<22>} = 7RT\sigma_{22} + \frac{2b^2}{3\rho}\left(\sigma_{12}^2 + \sigma_{22}^2 - 2\sigma_{11}^2 - 2\sigma_{11}\sigma_{22}\right) - \frac{28}{5}\frac{\mu}{\mathrm{Pr}\,p}\left(\frac{2}{3}RT\frac{\partial q_2}{\partial x_2} + \frac{2}{3}Rq_2\frac{\partial T}{\partial x_2} - \frac{2}{3}\frac{RTq_2}{\rho}\frac{\partial \rho}{\partial x_2} + \frac{5}{21}RT\sigma_{21}\frac{\partial u_1}{\partial x_2}\right), \tag{9.e}$$

$$\rho^{R13B}_{rrss} = 15\frac{p^2}{\rho} + \frac{4b^2}{\rho}\left(\sigma_{11}^2 + \sigma_{12}^2 + \sigma_{22}^2 + \sigma_{11}\sigma_{22}\right) - 8\frac{\mu}{\mathrm{Pr}\,p}\left(RT\frac{\partial q_2}{\partial x_2} + \frac{5}{2}Rq_2\frac{\partial T}{\partial x_2} - \frac{RTq_2}{\rho}\frac{\partial \rho}{\partial x_2} + RT\sigma_{12}\frac{\partial u_1}{\partial x_2}\right). \tag{9.f}$$

If we use accurate computational results from kinetic models (what we term here "*direct values*") for *all* moments in Eqs. (6), that is to say without considering any of the closure relations (7-9), then Eqs. (6) should be satisfied within the limits of computational error. This is because this set of equations is exact: no assumption or approximation is applied. Indeed, Eqs. (6.a-d), which state that u_2, σ_{12}, p_{22}, and $q_2 + u_1\sigma_{12}$ are constant in the whole domain at steady state, can be used to check whether the kinetic computational results are converged and at steady state or not [3, 32].

Verification of Eqs. (6.e-i) is more difficult, since this requires the calculation of derivatives. If a good expression for calculating the derivatives can be chosen, Eqs. (6.e-i) should also be satisfied if results from kinetic models are used. This is shown below.

3. Description of the test method

We rewrite Eqs. (6.e-i) as:

$$\sigma_{11} = -\frac{\mu}{p}\left(-\frac{4}{15}\frac{\partial q_2}{\partial x_2} + \frac{4}{3}\sigma_{21}\frac{\partial u_1}{\partial x_2} + \frac{\partial \rho_{<112>}}{\partial x_2} \right), \tag{10.a}$$

$$\sigma_{22} = -\frac{\mu}{p}\left(+\frac{8}{15}\frac{\partial q_2}{\partial x_2} - \frac{2}{3}\sigma_{21}\frac{\partial u_1}{\partial x_2} + \frac{\partial \rho_{<222>}}{\partial x_2} \right), \tag{10.b}$$

$$\sigma_{12} = -\frac{\mu}{p}\left(+\frac{2}{5}\frac{\partial q_1}{\partial x_2} + p\frac{\partial u_1}{\partial x_2} + \sigma_{22}\frac{\partial u_1}{\partial x_2} + \frac{\partial \rho_{<122>}}{\partial x_2} \right), \tag{10.c}$$

$$\begin{aligned} q_1 = &-\frac{\mu}{\mathrm{Pr}\,p}\left(-\frac{5}{2}RT\frac{\partial \sigma_{12}}{\partial x_2} - \frac{\sigma_{12}}{\rho}\frac{\partial p}{\partial x_2} - \frac{\sigma_{11}}{\rho}\frac{\partial \sigma_{12}}{\partial x_2} - \frac{\sigma_{12}}{\rho}\frac{\partial \sigma_{22}}{\partial x_2} \right) \\ &-\frac{\mu}{\mathrm{Pr}\,p}\left(+\frac{7}{5}q_2\frac{\partial u_1}{\partial x_2} + \frac{1}{2}\frac{\partial \rho_{rr<12>}}{\partial x_2} + \rho_{<112>}\frac{\partial u_1}{\partial x_2} \right), \end{aligned} \tag{10.d}$$

$$q_2 = -\frac{\mu}{\Pr p}\left(-\frac{5}{2}RT\frac{\partial p}{\partial x_2}-\frac{5}{2}RT\frac{\partial \sigma_{22}}{\partial x_2}-\frac{\sigma_{22}}{\rho}\frac{\partial p}{\partial x_2}-\frac{\sigma_{21}}{\rho}\frac{\partial \sigma_{12}}{\partial x_2}-\frac{\sigma_{22}}{\rho}\frac{\partial \sigma_{22}}{\partial x_2}\right) - \frac{\mu}{\Pr p}\left(+\frac{2}{5}q_1\frac{\partial u_1}{\partial x_2}+\frac{1}{2}\frac{\partial \rho_{rr<22>}}{\partial x_2}+\frac{1}{6}\frac{\partial \rho_{rrss}}{\partial x_2}+\rho_{<212>}\frac{\partial u_1}{\partial x_2}\right). \quad (10.e)$$

If a good expression for calculating derivatives is chosen, Eqs. (10) should be satisfied (within the limits of computational error) by the computational results of kinetic models for a particular flow problem. This is because Eqs. (10) are exact, without any assumption or approximation. In other words, if we use direct values of all moments in the right hand side of Eqs. (10), and calculate the derivatives accurately, our calculated values of σ_{ij} and q_i on the left hand side of Eqs. (10) should be the same as our *direct values* of σ_{ij} and q_i. We use this equality test as the basis for choosing the best technique for calculating derivatives in our tests.

All MCMs for rarefied gas flows involve some assumptions or approximations, e.g., the NSF is only the first order approximation in the Chapman-Enskog expansion. Therefore, if we use direct values of moments in MCM expressions for σ_{ij} and q_i, and use the same technique to calculate derivatives (e.g., Eqs. (3) for the NSF), our calculated σ_{ij} and q_i will not necessarily be equal to our direct values of σ_{ij} and q_i. The differences between these calculated values and direct values for different MCMs will not be the same as well. A smaller difference between these direct and calculated values implies a higher accuracy of the MCM under consideration. That is to say, we judge an MCM to be more physically realistic (at least for the flow considered) than another one when its calculated σ_{ij} and q_i are closer to the direct values. This is the fundamental idea behind the test method we propose here.

From this description, we can see that no boundary conditions for the MCMs are needed for these tests, no coupled governing equations are solved, but still a real flow involving the Knudsen layer can be considered. What is necessary, though, is to compute the direct values of the moments from an accurate solution of the microscopic kinetic equation.

For the first type of MCMs, introduced in Section 1, i.e. the NSF and Burnett equations, the expressions for σ_{ij} and q_i are explicit functions of density, velocity and temperature, and their spatial derivatives. These expressions can therefore be used directly in the tests. For the second type of MCMs, the governing equations for σ_{ij} and q_i are implicit, and must be transferred first into a form similar to Eqs. (10) in order to apply the test method. Furthermore, if some higher order moments are used in the expressions for σ_{ij} and q_i, e.g., $\rho_{<112>}$ in Eqs. (10), the direct values of the 13 moments (i.e., ρ, u_i, T, σ_{ij} and q_i) should be used in the closure relation of these higher order moments.

The parameters we use for our numerical tests are: the gas is argon; the temperature of both plates is 273 K; speed of plate 1 is zero; speed of plate 2 is as indicated in Table 1; initial molecule number density is 1.4×10^{20} m^{-3}; reference temperature is 273 K; viscosity at the reference temperature is 1.9552×10^{-5} kg/(m·s); molecular mass of argon is 6.63×10^{-26} kg. Table 1 shows the various one-dimensional steady Couette flows we considered for our tests. The "number of cells" in Table 1 indicates the number of finite volume cells in our kinetic model computation, which, as stated previously, is based on Mieussens' discrete velocity method [30-32] for the general ES-BGK model.

The relevant characteristic dimensionless numbers for these flows are the Mach number, the Reynolds number and the (global) Knudsen number, which are defined:

$$\mathrm{Ma} = \frac{u_{p2}}{a_p}, \qquad \mathrm{Re} = \frac{\rho_{ave} u_{p2} L}{\mu_{ref}}, \qquad \mathrm{Kn} = \frac{l}{L} \sim \frac{\mathrm{Ma}}{\mathrm{Re}}, \qquad l = \mu_{ref} \frac{\sqrt{RT_p}}{\rho_{ave} RT_p}, \tag{11}$$

where l is the molecular mean free path, u_{p2} is the speed of the moving plate, $a_p = \sqrt{5RT_p/3}$ is the sound speed at plate temperature T_p, L is the distance between the two plates, μ_{ref} is the viscosity of the gas at temperature T_p, and ρ_{ave} is the average mass density in the whole domain.

Once we obtain direct values of the moments from the kinetic model, it is important to find an appropriate way of calculating the spatial derivatives of these moments. We consider two ways of calculating the derivatives for the viscous stress, σ_{ij}, and heat flux, q_i, in Eqs. (10). These are:

- the classical three point formula [35] (central difference),

$$\left.\frac{dF}{dx}\right|_{x=x_i} = \frac{1}{2\Delta x}\left(F(x_{i+1}) - F(x_{i-1})\right), \tag{12}$$

  where function $F = F(x)$, and Δx is the regular spatial stepsize;

- the five point formula [35],

$$\left.\frac{dF}{dx}\right|_{x=x_i} = \frac{1}{12\Delta x}\left(F(x_{i-2}) - 8F(x_{i-1}) + 8F(x_{x+1}) - F(x_{i+2})\right) \ . \tag{13}$$

The first formula is second order accurate, while the second formula is third order accurate. Results using Eq. (12) were quite similar to results from Eq. (13), while the first is a simpler expression. Therefore, we choose the central difference formula, Eq. (12), to calculate all derivatives in our tests.

It should also be noted that if we calculate the viscous stress and heat flux in Eqs. (10) from the original computational results of kinetic theory including higher order moments, the calculated σ_{ij} and q_i have some small oscillations, and a jump in values adjacent to the boundaries. These oscillations in our calculated results show that the original computational results of kinetic theory do not seem to accurate enough for our test method, even though these results are quite good when the conservation laws are checked [3, 32]. The jumps adjacent to the boundaries in our calculated results come from the fact that there are inconsistencies immediately adjacent to the boundaries even in the original computational results of Mieussens' discrete velocity method [30-32]. These lead to a slight violation of the conservation laws due to numerical inaccuracy, and can be reduced when the grid spacing in the kinetic theory computations is reduced [3]. Note that in all the figures in this paper the values of viscous stress and heat flux adjacent to the walls are not shown because of these inconsistencies. Since results at those positions are needed in the calculation of spatial derivatives nearby, the calculated results from MCMs very near the walls, not only the nodes immediately adjacent to the walls, are not shown in all Figures.

In order to reduce these oscillations and jumps in the calculated data, while avoiding having to do time-consuming computation from the kinetic models again, we smooth the original computational results from the kinetic models by averaging over adjacent points (i.e., if the original number of cells used for the kinetic theory computation is *N*, the number of cells we use in our tests is *N*/2). We use this smoothed data, then, as the "direct values" in our calculations in the test. Consequently, oscillations and jumps in σ_{ij} and q_i calculated from Eqs. (10) are significantly decreased, while at the same time the cross-channel profile of the smoothed data still follows closely the profile of the original results from the kinetic models.

This can be seen in Figure 1, which shows the original results for σ_{11} in Case 2 of Table 1 using the ES-BGK kinetic model, with the σ_{11} calculated using Eqs. (10) with and without smoothing.

Therefore, we apply central differences for calculating derivatives, and smoothed data from the kinetic theory computation as direct values, for all our tests. The average relative error in the viscous stress between values calculated from Eqs. (10) with *all* direct data including higher order moments on the right hand side and the direct values is less than 0.01 in all test cases. Since the relative error becomes meaningless when a quantity approaches zero (as the heat flux does in the middle of the channel), we have not checked the average relative error in the heat flux.

4. Numerical results

Figures 2-13 show the direct values of σ_{ij} and q_i, and their calculated values from the NSF equations (3), the Burnett equations (4, 5), the Grad13 (7, 10), the R13A (8, 10), the R13B equations (9, 10). The test cases shown in the figures are Case 1 with the ES-BGK model, Case 7 with the ES-BGK model, and Case 6 with the ES-BGK model. Note that, since the profile of σ_{11} is similar to the profile of $-\sigma_{22}$, and no new information can be obtained from graphs of σ_{22}, graphs of σ_{22} are omitted in the figures.

The only difference between the Grad13, the R13A and the R13B equations for σ_{ij} and q_i in the tests is the way in which the higher order moments $\rho_{<ijk>}$, $\rho_{rr<ij>}$ and ρ_{rrss} in Eqs. (10) are calculated. A comparison of their calculated values using the Grad13, the R13A, the R13B equations and their direct values is discussed briefly in Appendix C.

The NSF equations are first order in Kn, the Burnett equations are second order in Kn, the Grad13 equations are between second and third order in Kn, the R13B equations are third order in Kn, and the R13A equations are between third and fourth order in Kn [4, 20]. Therefore, we would expect that at small Knudsen numbers the R13A and the R13B would give the best results, followed by the Grad13, the Burnett equations, and that the NSF equations would provide the worst results.

At small Kn numbers, such as in Case 1 (Figures 2-5), the calculated values of σ_{11}, σ_{22}, q_1 and q_2 give very good agreement with the direct data in the main part of the flow for all models except the NSF equations. Recall that the NSF equations do not account for any rarefaction effects on σ_{11}, σ_{22} and q_1, and, by Eqs. (3), predict their values as zero, while the direct values of these quantities are not zero even in the middle of the domain.

Results from the R13A and the R13B equations give the same profile across the channel as the direct values even near the boundary, while the Burnett equations differ in profile: if the curve from the R13A, the R13B and direct values is convex, then the corresponding curve from the Burnett equations is concave. The calculated values of σ_{12} from all MCMs in Case 1 are a good fit with the direct data in the centre of the channel, but not so good near the boundary. Therefore, as expected, at relatively small Knudsen numbers the R13A and the R13B equations give similar results; the next best model is the Grad13, followed by the Burnett equations. The NSF equations give the worst results.

When the Knudsen number increases, which means that the thickness of the Knudsen layer increases and the central part of the flow becomes smaller, none of the tested MCMs can be

said to be a suitable model for $\mathrm{Kn} > 0.1$. To our surprise, the calculated σ_{ij} and q_i from the R13A and the R13B equations have the opposite sign to the direct data, and also have a discontinuity near the boundaries when $\mathrm{Kn} > 0.1$, i.e., in Figures 10-13 for Case 6. (Note that this discontinuity disappears or can be neglected when $\mathrm{Kn} \le 0.1$, i.e. see Figures 2-5.) These two unusual phenomena are difficult to understand, and the reasons for them are still under investigation.

Generally, the calculated values of σ_{ij} and q_i from all sets of macroscopic equations fit the direct data well at small Knudsen numbers, but not so well at large Knudsen numbers. We suggest that the R13A or the R13B equations may be more appropriate as macroscopic continuum equations in rarefied gas flows with $\mathrm{Kn} \le 0.1$, and up to moderate Mach number. As the Knudsen number increases, and boundary effects dominate, all tested models fail, which can be attributed to their inability to properly describe non-equilibrium near solid surfaces. Note that the above discussion is independent of the kinetic models (BGK or ES-BGK) used in the tests.

Our observations here match those in the calculation of shock structures [19]: Burnett, Grad13, and R13A equations yield shock structures in agreement with DSMC computations for Mach numbers below about Ma=3.0, but not for higher Mach numbers, where rarefaction effects and deviations from equilibrium states become increasingly important.

5. Knudsen layers and the Knudsen number

Our numerical results show that, at least in this test method, all MCMs have difficulties in reproducing the data from the kinetic solution within the Knudsen layers. This warrants further discussion.

All MCMs discussed are related to the Knuden number as a smallness parameter: by their derivation, the NSF equations are exact within an error of the order $O(\mathrm{Kn}^2)$, the Burnett and Grad 13 moment equations are exact within an error of the order $O(\mathrm{Kn}^3)$, and the R13 equations are exact within an error of the order $O(\mathrm{Kn}^4)$. Based on this, we expect the differences between the kinetic solution and the solutions of the MCMs to be related to their respective errors, i.e. powers of the Knudsen number.

Normally, the Knudsen number is defined as the ratio between mean free path, l, and a relevant macroscopic length, L_{ref}: $\mathrm{Kn} = l/L_{ref}$. For the description of Couette flow, the intuitive choice for the macroscopic reference length is the channel width, L; which we do indeed use to define the Knudsen number in our numerical experiments. However, the failure of the MCMs to describe the Knudsen layers in our test indicates that this conventional definition of the Knudsen number (with the channel width) is appropriate to describe the bulk flow but not the Knudsen layers.

We may argue that, if the Knudsen layer is to be resolved, its thickness should be chosen as the reference length. Since the Knudsen layer has a thickness of the order of a molecular mean free path, this would imply $L_{ref}=l$, which results in a Knudsen number of order unity [4]. Then, none of the MCMs would be appropriate, since the basic requirement of their derivation — small Knudsen number — is not fulfilled.

Some researchers define a local Knudsen number that considers a reference length L_{loc} based on the steepness of gradients. In regions of steep gradients, the local length scale can be considerably smaller than the channel width ($L_{loc}<<L$), and this would result in a higher

relevant Knudsen number $\mathrm{Kn}_{loc} = l/L_{loc}$>>Kn. A common definition of the local reference length uses the density gradient [29, 36]

$$L_{loc} = \frac{\rho}{d\rho/dx} \ . \tag{14}$$

For the numerical data in our test cases, the local length defined by Eq. (14) turns out to be larger than the channel width, and thus would lead to Knudsen numbers well below the Knudsen number based on the channel width. In any case, the length definition given by Eq. (14) is not well suited, since it relates a quantity that does not vanish in equilibrium (the density) to a non-equilibrium quantity (the density gradient). So for linear processes, where gradients are small, the corresponding lengthscale would be very large. Knudsen layers can be considered as linear phenomena [4, 25, 26], and thus the length scale defined by Eq. (14) is not suitable to identify Knudsen layers. The same holds true for dispersion and damping of ultrasonic sound waves.

Thus, the local reference length scale must be defined differently, but presently it is unclear what definition would be a proper choice. In any case, one will expect that the local Knudsen number should be larger in regions of large gradients, in particular within the Knudsen layers.

6. Critique of the testing method

In this section we take a critical look at our proposed test method. For this discussion we need to distinguish between three sets of values for the moments:

(a) the direct values, which result from the solution of the kinetic equation, $\phi^D = \left\{\rho^D, u_i^D, T^D, \sigma_{ij}^D, q_i^D\right\}$;

(b) the hypothetical solution of the MCMs with reliable boundary conditions, $\phi^H = \left\{\rho^H, u_i^H, T^H, \sigma_{ij}^H, q_i^H\right\}$;

(c) the values computed from our test, $\phi^T = \{\sigma_{ij}^T, q_i^T\}$, which use the MCM equations together with the direct values, ϕ^D. In this case, the direct values for ρ, u_i, T are used for both types of MCMs. For MCMs of the first type, stress and heat flux are computed in the test, while the test for the second type of MCMs computes the test values for stress and heat flux by means of the complete set of moments from the kinetic solution, including stress and heat flux.

We emphasize that the proper test for quality of an MCM should be a comparison of the direct values, ϕ^D, to the full numerical solution of the MCM, ϕ^H, but this route is not accessible while the boundary conditions are not known. Instead, our test method compares the direct values, ϕ^D, with the test values, ϕ^T, and so the question arises whether an insufficient agreement between ϕ^D and ϕ^T implies an insufficient agreement between ϕ^D and ϕ^H.

In our test the hydrodynamic variables ρ, u_i, and T are given by the kinetic solution, and only the test values for σ_{ij} and q_i differ from the kinetic solution. In contrast, in the full numerical solution of the MCM, the values of *all* variables will be different from the accurate kinetic result. This difference leads to the question whether the variance between the kinetic results and the full numerical solution can be smaller than the variance between the kinetic results and test values. Indeed, in the test method some of the variables are forced to follow the kinetic solution, and that might lead to a larger variance for the remaining variables [37].

From the discussion of the preceeding section, we expect that all differences between MCMs and the kinetic solutions are related to the (local) Knudsen number. Accordingly, in a proper dimensionless formulation, the absolute differences from the kinetic solution (i.e. the direct

values) should be related to (powers of) the Knudsen number for *all* variables. This should be so for the test values as well as for the hypothetical full solution.

It is possible that the absolute differences are, in fact, less important than relative differences. If the absolute values of two variables differ, but the absolute error in those values has the same size, then the relative errors can be quite different. We recall that (as can be seen, e.g., from the Burnett equations, Eqs (4-5)) ρ, u_i, and T are equilibrium quantities that will be larger than σ_{12}, q_2, which are of first order in the Knudsen number. For Couette flow, σ_{11}, σ_{22}, and q_1 are even smaller (second order in Kn). The higher order MCMs lead to corrections of the values for all variables, and the relative importance of the corrections is more marked for those moments that are "small" (σ_{12}, q_2) or very small (σ_{11}, σ_{22}, q_1) [4].

In our test method we use direct values of ρ, u_i, and T and force all deviations from the direct values on σ_{12}, q_2, σ_{11}, σ_{22}, q_1. It is quite likely that the overall relative error for all variables could be smaller, by forcing some deviation on the equilibrium variables ρ, u_i, and T. This would allow us to reduce the relative errors in the non-equilibrium variables (which are large in the current tests), that might then result in small relative errors for ρ, u_i, T. It is not clear, however, how this could be done technically, and we have not attempted this here.

From this discussion we suggest that our test method paints a bleaker picture of the quality of MCMs than may be the case. Indeed, in [4] the Couette flow problem was considered in a semi-analytic way by a superposition of a non-linear "bulk solution" and linear Knudsen layers, whose amplitude was adjusted to fit DSMC data. This allowed a matching of the non-

equilibrium variables (σ_{12}, q_2, σ_{11}, σ_{22}, q_1) quite well (for Kn=0.1), while discrepancies were forced on ρ, u_i, and T where the relative errors are comparatively small.

In summary, we propose that our presented test method can give important insight into the behavior of MCMs, but the full solution of the MCMs (with proper boundary conditions currently unknown) would certainly be a more comprehensive approach.

7. Conclusions

Many Macroscopic Continuum Models (MCMs) have been proposed for rarefied gas flows. No single model is commonly accepted, especially for gas microfluidics where the Knudsen layer is important and the gas rarefied even at normal pressure. For computational efficiency, MCMs would, however, be preferred over kinetic models or the DSMC for rarefied gas flows as long as a physically accurate and numerically tractable model can be found. Unfortunately this question cannot yet be answered, for the boundary conditions of MCMs, except for the conventional NSF equations, are still under development.

The aim of our test method proposed in this paper is to contribute towards an answer to the question of which macroscopic model is suitable for gas microfluidics. The characteristics of our test method are: it does not require boundary conditions in the calculations and comparison; coupled governing equations need not be solved; full (non linear) expressions are considered; the solution of the same flow using a kinetic equation is required.

As the first application of this test method, the NSF equations, Burnett equations, Grad's 13 moment equations, the original Regularized 13 moment equations (R13A), and the Regularized 13 moment equations from an order of magnitude approach (R13B) are

investigated for their ability to describe one-dimensional steady Couette flow accurately. For relatively low Knudsen numbers ($\mathrm{Kn} \leq 0.1$) in the transition-continuum regime, it is found that the two types of R13 equations give results similar to each other, which are better than results from Grad's 13 moment equations, which however give better results than the Burnett equations. The NSF equations give the worst results in comparison. This, in fact, is as expected from the order of accuracy in the Knudsen number of these MCMs.

For large Knudsen numbers (Kn>0.1), all MCMs we tested fail to describe the flow with acceptable accuracy. Problems in describing Knudsen layers, as well as previous work on strong shock structures, indicates there may be severe limitations on the applicability of some current MCMs for rarefied gas flows. In particular, the failure of MCMs in the vicinity of the wall can be attributed to the large local Knudsen number, so that models that were derived under the assumption of small Knudsen number lose validity. The proper definition of the local Knudsen number is unclear, although a deeper discussion of this question is outside the scope of this paper.

While we have examined one dimensional steady Couette flow in this paper, other benchmark flow problems should be considered in the future.

Acknowledgments

This research was supported by the Natural Sciences and Engineering Research Council (NSERC) of Canada. YZ would also like to thank the Leverhulme Trust in the UK for support under Postdoctoral Visiting Fellowship F/00273/E. Moreover, the authors would like to thank the two anonymous referees for their valuable comments.

Appendix A: A brief description of relevant kinetic theory

In the microscopic theory of rarefied gas dynamics, the state variable is the distribution function $f(\mathbf{x},\mathbf{c},t)$, which specifies the density of microscopic particles with velocity **c** at time *t* and position **x** [2-6]. The particles, which can be thought of as idealized atoms, move freely in space unless they undergo collisions. The corresponding evolution of *f* is described by the Boltzmann equation [2, 4], which, when external forces are omitted, is written as

$$\frac{\partial f}{\partial t} + c_i \frac{\partial f}{\partial x_i} = S(f)\,. \tag{A.1}$$

Here, the first term on the left hand side describes the local change of *f* with time and the second term is the convective change of *f* due to the microscopic motion of the gas particles. The term on the right hand side, $S(f)$, describes the change of *f* due to collisions among particles. For a monatomic gas the collision term reads

$$S(f) = \int \left(f' f'^{1} - f f^{1}\right) \sigma g \sin\theta \, d\theta \, d\varepsilon \, d\mathbf{c}^{\mathbf{1}}\,, \tag{A.2}$$

where the superscript 1 denotes parameters for particle 1 (which is the collision partner of the particle considered), the superscript $'$ denotes parameters for the state after collision, $g = \left|\mathbf{c} - \mathbf{c}^{\mathbf{1}}\right|$ is the relative speed of the colliding particles, σ is the scattering factor, and ε and θ are the angles of collision.

In kinetic models, the Boltzmann collision term, $S(f)$, is replaced by a relaxation expression which is typically of the form

$$S_m(f) = -\nu\left(f - f_{ref}\right). \tag{A.3}$$

Here, f_{ref} is a suitable reference distribution function, and ν is the (mean) collision frequency; the various kinetic models differ in their choices for f_{ref} and ν. A detailed comparison of kinetic models is presented in [3, 4, 32].

The BGK model [4, 32, 33] is the simplest kinetic model, where the reference function is simply the Maxwellian,

$$f_{ref} = f_M = \frac{\rho}{m}\sqrt{\left(\frac{1}{2\pi RT}\right)^3}\cdot\exp\left(-\frac{C^2}{2RT}\right), \tag{A.4}$$

and its evaluation in the hydrodynamic limit yields (see, e.g., [4])

$$\mu = \frac{p}{\nu}, \qquad \kappa = \frac{5}{2}\frac{pR}{\nu}, \qquad \mathrm{Pr} = 1. \tag{A.5}$$

While this model is widely used for theoretical considerations, it gives the wrong value ($\mathrm{Pr} = 1$) for the Prandtl number. More recent models have been proposed to correct this failure.

The ES-BGK model [4, 7, 32, 34], replaces the Maxwellian with a generalized Gaussian, so that

$$f_{ref} = f_{ES} = \rho\cdot\left(\det\left(2\pi\lambda_{ij}\right)\right)^{-1/2}\cdot\exp\left(-\frac{1}{2}C_i\varepsilon_{ij}C_j\right), \tag{A.6}$$

and it yields

$$\mu = \frac{1}{1-b}\frac{p}{\nu}, \quad \kappa = \frac{5}{2}\frac{pR}{\nu}, \qquad \mathrm{Pr} = \frac{1}{1-b}. \tag{A.7}$$

The matrix $\boldsymbol{\lambda}$ is defined as

$$\lambda_{ij} = RT\delta_{ij} + b\,\sigma_{ij}/\rho = (1-b)RT\delta_{ij} + b\,p_{ij}/\rho, \tag{A.8}$$

where b is a number that serves to adjust the Prandtl number, δ_{ij} is the unit matrix, and $\boldsymbol{\varepsilon}$ is the inverse of the tensor $\boldsymbol{\lambda}$. The value of b must be in the interval $[-1/2, 1]$ to ensure that λ_{ij} is positive definite, which ensures the integrability of f_{ES}.

Appendix B: MCM equations in three dimensions

B.1. NSF and Burnett equations for the BGK and ES-BGK models

The Knudsen number, Kn, is normally defined as the ratio of the gas molecular mean free path to the relevant macroscopic length scale of the problem, e.g. the channel width in our Couette flow problem. The viscous stress, σ_{ij}, and heat flux, q_i, for the NSF equations are obtained from the Chapman-Enskog (CE) expansion technique to first order in the Kn, while the expressions for the Burnett equations are obtained at second order in the CE expansion. For details of the CE technique, see [4-6]; here, only the final expressions are listed.

The viscous stress and heat flux at first order, the NSF order, are given by

$$\sigma_{ij}^{NSF} = -2\mu \frac{\partial u_{<i}}{\partial x_{j>}}, \qquad q_i^{NSF} = -\kappa \frac{\partial T}{\partial x_i}, \tag{B.1}$$

where μ is the viscosity and κ is the thermal conductivity.

Equivalent Burnett expressions, calculated using the general ES-BGK model, are [3, 7]

$$\sigma_{ij}^{B} = -2\mu \frac{\partial u_{<i}}{\partial x_{j>}} + \frac{\mu^2}{p^2}\Phi_{ij}, \qquad q_i^{B} = -\kappa \frac{\partial T}{\partial x_i} + \frac{\mu^2}{p^2 \,\mathrm{Pr}} \cdot \Gamma_i, \tag{B.2}$$

where

$$\begin{aligned} \Phi_{ij} = & -2R^2T^2 \frac{\partial^2 \rho}{\partial x_{<i} \partial x_{j>}} - 2b\rho R^2 T \frac{\partial^2 T}{\partial x_{<i} \partial x_{j>}} + \frac{2R^2T^2}{\rho} \frac{\partial \rho}{\partial x_{<i}} \frac{\partial \rho}{\partial x_{j>}} \\ & - 2R^2 T \frac{\partial T}{\partial x_{<i}} \frac{\partial \rho}{\partial x_{j>}} + 2p \frac{\partial u_{<i}}{\partial x_k} \frac{\partial u_{j>}}{\partial x_k} + \frac{2-4\omega}{3} p \frac{\partial u_{<i}}{\partial x_{j>}} \frac{\partial u_k}{\partial x_k} \\ & + 2\omega(1-b)\rho R^2 \frac{\partial T}{\partial x_{<i}} \frac{\partial T}{\partial x_{j>}}, \end{aligned} \tag{B.3.a}$$

$$\Gamma_i = \frac{5b-4}{3} pRT \frac{\partial^2 u_j}{\partial x_i \partial x_j} + pRT \frac{\partial^2 u_i}{\partial x_j \partial x_j} - 2R^2 T^2 \frac{\partial u_{<j}}{\partial x_{i>}} \frac{\partial \rho}{\partial x_j}$$
$$+ \left(6 + \omega - \frac{7}{2} b\right) pR \frac{\partial u_i}{\partial x_j} \frac{\partial T}{\partial x_j} + \left(1 + \omega + \frac{3}{2} b\right) pR \frac{\partial u_j}{\partial x_i} \frac{\partial T}{\partial x_j} \qquad \text{(B.3.b)}$$
$$+ \frac{1}{6}\left[(-13 - b) + (14 - 10b)(1 - \omega)\right] pR \frac{\partial u_j}{\partial x_j} \frac{\partial T}{\partial x_i},$$

with $b = 1 - (1/\mathrm{Pr})$. Eqs. (B.2-B.3) simplify to the Burnett equations for the traditional BGK model when $b = 0$ [7]. In the above, ω is the power index (a positive number of order unity) used in the following expression for the gas viscosity, μ, as a function of temperature [5]:

$$\mu(T) = \mu_0 \left(\frac{T}{T_0}\right)^{\omega}, \qquad \text{(B.4)}$$

where μ_0 is the viscosity at a reference temperature T_0. Maxwellian gas molecules have $\omega = 1$, which are used in our numerical simulations. The expressions for σ_{ij}^B and q_i^B in Eqs. (B.2-B.3) are irreducible forms in terms of the gradients of density, velocity, and temperature.

B.2. Grad13, R13A and R13B equations for the BGK and ES-BGK models

There are 13 unknown variables, and 13 moment equations in the Grad13, R13A and R13B models for a three-dimensional problem. The independent variables are: ρ, u_1, u_2, u_3, T, σ_{11}, σ_{22}, σ_{12}, σ_{13}, σ_{23}, q_1, q_2 and q_3; while other variables can be derived from these quantities, such as $p = \rho RT$, $\sigma_{33} = -(\sigma_{11} + \sigma_{22})$, $\sigma_{21} = \sigma_{12}$, $\sigma_{31} = \sigma_{13}$, $\sigma_{32} = \sigma_{23}$.

The Grad13 and the R13A equations for the general ES-BGK model are obtained along the same lines as the corresponding equations for the Boltzmann equation with Maxwellian gas molecules [4, 18]. Here, only some steps in the derivation are shown; see [3, 4, 18] for more details.

After multiplying the kinetic equation by polynomials of the peculiar velocity, viz. 1, C_i, C^2, $C_{<i}C_{j>}$ and $C^2C_i/2$, and then integrating over velocity space, the basic 13 moment equations for the general ES-BGK model are obtained [3,4]

$$\frac{\partial \rho}{\partial t}+\rho\frac{\partial u_k}{\partial x_k}+u_k\frac{\partial \rho}{\partial x_k}=0\,, \tag{B.5.a}$$

$$\rho\frac{\partial u_i}{\partial t}+\rho u_k\frac{\partial u_i}{\partial x_k}+\frac{\partial p}{\partial x_i}+\frac{\partial \sigma_{ik}}{\partial x_k}=0\,, \tag{B.5.b}$$

$$\frac{3}{2}\rho R\frac{\partial T}{\partial t}+\frac{3}{2}\rho R u_k\frac{\partial T}{\partial x_k}+\frac{\partial q_k}{\partial x_k}+p\frac{\partial u_k}{\partial x_k}+\sigma_{ik}\frac{\partial u_i}{\partial x_k}=0\,, \tag{B.5.c}$$

$$\frac{\partial \sigma_{ij}}{\partial t}+\frac{\partial\left(\sigma_{ij}u_k\right)}{\partial x_k}+\frac{4}{5}\frac{\partial q_{<i}}{\partial x_{j>}}+2p\frac{\partial u_{<i}}{\partial x_{j>}}+2\sigma_{k<i}\frac{\partial u_{j>}}{\partial x_k}+\frac{\partial \rho_{<ijk>}}{\partial x_k}=-\frac{p}{\mu}\sigma_{ij}\,, \tag{B.5.d}$$

$$\begin{aligned}&\frac{\partial q_i}{\partial t}+\frac{\partial\left(q_iu_k\right)}{\partial x_k}-\frac{5}{2}RT\frac{\partial p}{\partial x_i}-\frac{5}{2}RT\frac{\partial \sigma_{ik}}{\partial x_k}-\frac{\sigma_{ik}}{\rho}\frac{\partial p}{\partial x_k}-\frac{\sigma_{ij}}{\rho}\frac{\partial \sigma_{jk}}{\partial x_k}+\frac{7}{5}q_k\frac{\partial u_i}{\partial x_k}\\&\quad+\frac{2}{5}q_k\frac{\partial u_k}{\partial x_i}+\frac{2}{5}q_i\frac{\partial u_k}{\partial x_k}+\frac{1}{2}\frac{\partial \rho_{rr<ik>}}{\partial x_k}+\frac{1}{6}\frac{\partial \rho_{rrss}}{\partial x_i}+\rho_{<ijk>}\frac{\partial u_j}{\partial x_k}=-\frac{\Pr p}{\mu}q_i\,,\end{aligned} \tag{B.5.e}$$

with the definition of the moments as in Eqs. (1). Equations (B.5) simplify to a similarly basic 13 moment equation set for the BGK model when we make Pr=1 [3, 4, 32]. Equations (B.5.a-B.5.c) are, in fact, the non-conservative form of Eqs. (2). Note that Eqs. (B.5) do not form a closed set of equations for the 13 variables, since they contain the higher order moments $\rho_{<ijk>}$, $\rho_{rr<ik>}$ and ρ_{rrss}. In the Grad13 equations from the general ES-BGK model, these are given as [4, 8]

$$\rho^{G13}_{<ijk>}=0\,,\qquad \rho^{G13}_{rr<ij>}=7RT\sigma_{ij}\,,\qquad \rho^{G13}_{rrss}=15\frac{p^2}{\rho}\,. \tag{B.6}$$

In the R13A equations from the general ES-BGK model, we have the following expressions for the higher order moments [3, 4, 18]

$$\rho^{R13A}_{<ijk>}=-3\frac{\mu}{\Pr p}\left(RT\frac{\partial \sigma_{<ij}}{\partial x_{k>}}-\frac{RT}{\rho}\sigma_{<ij}\frac{\partial \rho}{\partial x_{k>}}+\frac{4}{5}q_{<i}\frac{\partial u_j}{\partial x_{k>}}-\frac{\sigma_{<ij}}{\rho}\frac{\partial \sigma_{k>l}}{\partial x_l}\right), \tag{B.7.a}$$

$$\rho_{rr<ij>}^{R13A} = 7RT\sigma_{ij} - \frac{28}{5}\frac{\mu}{\Pr\, p}\left(RT\frac{\partial q_{<i}}{\partial x_{j>}} + Rq_{<i}\frac{\partial T}{\partial x_{j>}} - \frac{RTq_{<i}}{\rho}\frac{\partial \rho}{\partial x_{j>}} - \frac{q_{<i}}{\rho}\frac{\partial \sigma_{j>k}}{\partial x_k}\right)$$
$$- \frac{28}{5}\frac{\mu}{\Pr\, p}\left(-\frac{5}{6}\frac{\sigma_{ij}}{\rho}\frac{\partial q_k}{\partial x_k} - \frac{5}{6}\frac{\sigma_{ij}}{\rho}\sigma_{kl}\frac{\partial u_k}{\partial x_l}\right) \qquad \text{(B.7.b)}$$
$$- \frac{28}{5}\frac{\mu}{\Pr\, p}\left(\frac{5}{7}RT\left(\sigma_{k<i}\frac{\partial u_{j>}}{\partial x_k} + \sigma_{k<i}\frac{\partial u_k}{\partial x_{j>}} - \frac{2}{3}\sigma_{ij}\frac{\partial u_k}{\partial x_k}\right)\right),$$

$$\rho_{rrss}^{R13A} = 15\frac{p^2}{\rho}$$
$$- 8\frac{\mu}{\Pr\, p}\left(RT\frac{\partial q_k}{\partial x_k} + \frac{5}{2}Rq_k\frac{\partial T}{\partial x_k} - \frac{RTq_k}{\rho}\frac{\partial \rho}{\partial x_k} - \frac{q_i}{\rho}\frac{\partial \sigma_{ik}}{\partial x_k} + RT\sigma_{ik}\frac{\partial u_i}{\partial x_k}\right). \qquad \text{(B.7.c)}$$

In the R13B equations from the general ES-BGK model, the expressions for higher order moments are similar to Eqs. (B.7), but some higher order terms are removed and non-linear terms in the production terms (which have been omitted in [3]) are accounted for, i.e.

$$\rho_{<ijk>}^{R13B} = -3\frac{\mu}{\Pr\, p}\left(RT\frac{\partial \sigma_{<ij}}{\partial x_{k>}} - \frac{RT}{\rho}\sigma_{<ij}\frac{\partial \rho}{\partial x_{k>}} + \frac{4}{5}q_{<i}\frac{\partial u_j}{\partial x_{k>}}\right), \qquad \text{(B.8.a)}$$

$$\rho_{rr<ij>}^{R13B} = 7RT\sigma_{ij} + \frac{2b^2}{\rho}\sigma_{r<i}\sigma_{j>r} - \frac{28}{5}\frac{\mu}{\Pr\, p}\left(RT\frac{\partial q_{<i}}{\partial x_{j>}} + Rq_{<i}\frac{\partial T}{\partial x_{j>}} - \frac{RTq_{<i}}{\rho}\frac{\partial \rho}{\partial x_{j>}}\right)$$
$$- \frac{28}{7}\frac{\mu RT}{\Pr\, p}\left(\sigma_{k<i}\frac{\partial u_{j>}}{\partial x_k} + \sigma_{k<i}\frac{\partial u_k}{\partial x_{j>}} - \frac{2}{3}\sigma_{ij}\frac{\partial u_k}{\partial x_k}\right), \qquad \text{(B.8.b)}$$

$$\rho_{rrss}^{R13B} = 15\frac{p^2}{\rho} + \frac{2b^2}{\rho}\sigma_{rs}\sigma_{sr}$$
$$- 8\frac{\mu}{\Pr\, p}\left(RT\frac{\partial q_k}{\partial x_k} + \frac{5}{2}Rq_k\frac{\partial T}{\partial x_k} - \frac{RTq_k}{\rho}\frac{\partial \rho}{\partial x_k} + RT\sigma_{ik}\frac{\partial u_i}{\partial x_k}\right), \qquad \text{(B.8.c)}$$

where $b = 1 - (1/\Pr)$ in the general ES-BGK model. Eqs. (B.7-B.8) simplify to the corresponding expressions for the BGK model when Pr=1 [3, 4].

Appendix C: Discussion on higher order moments $\rho_{<ijk>}$, $\rho_{rr<ij>}$, and ρ_{rrss}

In this Appendix we briefly discuss the values of higher moments that appear in the MCM equations. We found that the computed values of the moments $\rho_{rr<22>}$ from the Grad13 equations fit the data from the kinetic model better than, or at least similar to, results from the R13A and the R13B equations for all test cases. While for $\rho_{<ijk>}$ and ρ_{rr12}, the opposite is the case, that is the R13A and R13B equations give better results than the Grad13 equations. At small Knudsen numbers or small plate velocities, the computed values of ρ_{rrss} from the Grad13, the R13A and the R13B equations fit the original data very well; however they are not so good when Kn or the plate velocity is large. The computed ρ_{rrss} from the Grad13, R13A and R13B equations do not fit the original data. There is no apparent way of deciding which one of the R13A and R13B equation sets is better. As an example, Figure 14 shows the comparison of calculated $\rho_{<112>}$ with its *direct* values from the BGK model in case 1 (Kn=0.025, Ma=0.975).

As a general comment we add that higher moments are more difficult to match, since they reflect on higher order deviations from equilibrium. Their exact values are less important, since they are not representing meaningful physical quantities. What is important is their influence on the meaningful quantities (such as density, temperature, velocity, stress, heat flux), as manifested in the moment equations.

References

[1] G. E. Karniadakis and A. Beskok, Micro Flows: Fundamentals and Simulation, Springer-Verlag New York, Inc., 2002.

[2] C. Cercignani, Rarefied Gas Dynamics: From Basic Concepts to Actual Calculations, Cambridge University Press, 2000.

[3] Y. Zheng, Analysis of kinetic models and macroscopic continuum equations for rarefied gas dynamics, Ph.D thesis, Dept. Mech. Eng., Univ. of Victoria, Canada, 2004.

[4] H. Struchtrup, Macroscopic transport Equations for Rarefied Gas Flows—Approximation Methods in Kinetic Theory, Interaction of Mechanics and Mathematics Series, Springer, Heidelberg, 2005.

[5] M. N. Kogan, Rarefied Gas Dynamics, Plenum Press, 1969.

[6] S. Chapman and T. G. Cowling, The Mathematical Theory of Non-uniform Gases, Third Edition, Cambridge Univerisity Press, 1970.

[7] Y. Zheng and H. Struchtrup, Burnett equations for the ellipsoidal statistical BGK model, Continuum Mech. Thermodyn. 16 (2004) 97.

[8] H. Grad, Principles of the kinetic theory of gases, Handbuch der Physik XII (1958) 205.

[9] X. Zhong, R. W. MacCormack and D. R. Chapman, Stabilization of the Burnett equations and application to hypersonic flows, AIAA J. 31 (1993) 1036.

[10] X. Chen, H. Rao and E. Spiegel, Continuum description of rarefied gas dynamics. I. Derivation from kinetic theory, Phys. Rev. E 64 (2001) 046308.

[11] E. Spiegel and J. Thiffeault, Higher-order continuum approximation for rarefied gases, Phys. Fluids 15 (2003) 3558.

[12] S. Jin and M. Slemrod, Regularization of the Burnett equations via relaxation, J. Stat. Phys. 103 (2001) 1009.

[13] S. Jin, L. Pareschi and M. Slemrod, A relaxation scheme for solving the Boltzmann equation based on the Chapman-Enskog expansion, Acta Math. Appl. Sin. (English Series) 18 (2002) 37.

[14] C. D. Levermore, Moment closure hierarchies for kinetic theories, J. Stat. Phys. 83 (1996) 1021.

[15] E. V. Volpe and D. Baganoff, Maximum entropy pdfs and the moment problem under near-Gaussian conditions, Probabilistic Eng. Mech. 18 (2003) 17.

[16] R. S. Myong, A generalized hydrodynamic computational model for rarefied and microscale diatomic gas flows, J. Comput. Phys. 195 (2004) 655.

[17] I. Müller, D. Reitebuch and W.Weiss, Extended thermodynamics – consistent in order of magnitude, Continuum Mech. Thermodyn. 15 (2002) 113.

[18] H. Struchtrup and M. Torrilhon, Regularization of Grad's 13 moment equations: Derivation and linear analysis, Phys. Fluids 15 (2003) 2668.

[19] M. Torrilhon and H. Struchtrup, Regularized 13-Moment equations: shock structure calculations and comparison to Burnett models, J. Fluid Mech. 513 (2004) 171.

[20] H. Struchtrup, Stable transport equations for rarefied gases at high orders in the Knudsen number, Phys. Fluids 16 (2004) 3921.

[21] H. Struchtrup, Derivation of 13 moment equations for rarefied gas flow to second order accuracy for arbitrary interaction potentials, Multiscale Model. Simul. 3 (2005) 221.

[22] D. A. Lockerby, J. M. Reese and M. A. Gallis, Capturing the Knudsen layer in continuum-fluid models of nonequilibrium gas flows, AIAA J. 43 (2005) 1391.

[23] J. M. Reese, L. C. Woods, F. J. P. Thivet and S. M. Candel, A second-order description of shock structure, J. Comput. Phys. 117 (1995) 240.

[24] A. V. Bobylev, The Chapman-Enskog and Grad methods for solving the Boltzmann equation, Sov. Phys. Dokl. 27 (1982) 29.

[25] H. Struchtrup, Failures of the Burnett and super-Burnett equations in steady state processes, Cont. Mech. Thermodyn. 17 (2005) 43.

[26] D. A. Lockerby, J. M. Reese and M. A. Gallis, The usefulness of higher-order constitutive relations for describing the Knudsen layer, Phys. Fluids 17 (2005) 100609.

[27] T. Thatcher, Microscale gas flow: A comparison of Grad's 13 moment equations and other continuum approaches, Masters Thesis, Dept. Mech. Eng., Univ. of Victoria, Canada, 2005.

[28] Y. Sone, Kinetic Theory and Fluid Dynamics. Birkhauser Boston, 2002.

[29] G. A. Bird, Molecular Gas Dynamics and the Direct Simulation of Gas Flows, Oxford Science Publications, Oxford, 1994.

[30] L. Mieussens, Discrete-velocity models and numerical schemes for the Boltzmann-BGK equation in plane and axisymmetric geometries, J. Comput. Phys. 162 (2000) 429.

[31] L. Mieussens and H. Struchtrup, Numerical comparison of BGK-models with proper Prandtl number, Phys. Fluids 16 (2004) 2797.

[32] Y. Zheng and H. Struchtrup, Ellipsoidal statistical Bhatnagar-Gross-Krook model with velocity-dependent collision frequency, Phys. Fluids 17 (2005) 127103.

[33] P.L. Bhatnagar, E.P. Gross and M. Krook, A model for collision processes in gases. I: small amplitude processes in charged and neutral one-component systems", Phys. Rev. 94 (1954) 511.

[34] J. Lowell H. Holway, New statistical models for kinetic theory: methods of construction, Phys. Fluids 9 (1966) 1658.

[35] R. L. Burden and J. D. Faires, Numerical Analysis, Sixth Edition, Brooks/Cole Publishing Company, 1997.

[36] M. Gad-el-Hak, The fluid mechanics of microdevices – The Freeman Scholar lecture, J. Fluids Eng. 121 (1999) 5.

[37] This important question was posed by one of the anonymous referees.

List of Figure captions

Figure 1: Cross-Channel Couette flow profile of σ_{11} in Case 2 (Kn=0.1, Ma=0.975); original values from the ES-BGK model and calculated values from Eqs. (10), with and without smoothing.

Figure 2: Cross-channel Couette flow profile of σ_{11}; direct values from the ES-BGK model and corresponding calculated values from indicated sets of macroscopic equations; Case 1 (Kn=0.025, Ma=0.975).

Figure 3: Cross-channel Couette flow profile of σ_{12}; direct values from the ES-BGK model and corresponding calculated values from indicated macroscopic sets of macroscopic equations; Case 1 (Kn=0.025, Ma=0.975).

Figure 4: Cross-channel Couette flow profile of q_1; direct values from the ES-BGK model and corresponding calculated values from indicated sets of macroscopic equations; Case 1 (Kn=0.025, Ma=0.975).

Figure 5: Cross-channel Couette flow profile of q_2; direct values from the ES-BGK model and corresponding calculated values from indicated sets of macroscopic equations; Case 1 (Kn=0.025, Ma=0.975).

Figure 6: Cross-channel Couette flow profile of σ_{11}; direct values from the ES-BGK model and corresponding calculated values from indicated sets of macroscopic equations; Case 7 (Kn=0.1, Ma=1.950).

Figure 7: Cross-channel Couette flow profile of σ_{12}; direct values from the ES-BGK model and corresponding calculated values from indicated sets of macroscopic equations; Case 7 (Kn=0.1, Ma=1.950).

Figure 6: Cross-channel Couette flow profile of σ_{11}; direct values from the ES-BGK model and corresponding calculated values from indicated sets of macroscopic equations; Case 7 (Kn=0.1, Ma=1.950).

Figure 9: Cross-channel Couette flow profile of q_2; direct values from the ES-BGK model and corresponding calculated values from indicated sets of macroscopic equations; Case 7 (Kn=0.1, Ma=1.950).

Figure 10: Cross-channel Couette flow profile of σ_{11}; direct values from the ES-BGK model and corresponding calculated values from indicated sets of macroscopic equations; Case 6 (Kn=0.5, Ma=3.251).

Figure 11: Cross-channel Couette flow profile of σ_{12}; direct values from the ES-BGK model and corresponding calculated values from indicated sets of macroscopic equations; Case 6 (Kn=0.5, Ma=3.251).

Figure 12: Cross-channel Couette flow profile of q_1; direct values from the ES-BGK model and corresponding calculated values from indicated sets of macroscopic equations; Case 6 (Kn=0.5, Ma=3.251).

Figure 13: Cross-channel Couette flow profile of q_2; direct values from the ES-BGK model and corresponding calculated values from indicated sets of macroscopic equations; Case 6 (Kn=0.5, Ma=3.251).

Figure 14: Cross-channel Couette flow profile of ρ_{rr12}; direct values from the BGK model and corresponding calculated values from indicated sets of macroscopic equations; Case 1 (Kn=0.025, Ma=0.975).

Table 1: One-dimensional steady Couette flows used in the tests

Case	Knudsen number	Plate speed (m/s)	Domain width (mm)	Mach number	Reynolds number	Number of cells
1	0.025	300.0	353.3	0.975	50.345	200
2	0.1	300.0	88.33	0.975	12.587	100
3	0.5	300.0	17.67	0.975	2.518	100
4	1.0	300.0	8.833	0.975	1.259	50
5	0.5	600.0	17.67	1.950	5.036	100
6	0.5	1000.0	17.67	3.251	8.393	100
7	0.1	600.0	88.33	1.950	25.174	100
8	0.1	1000.0	88.33	3.251	41.970	100

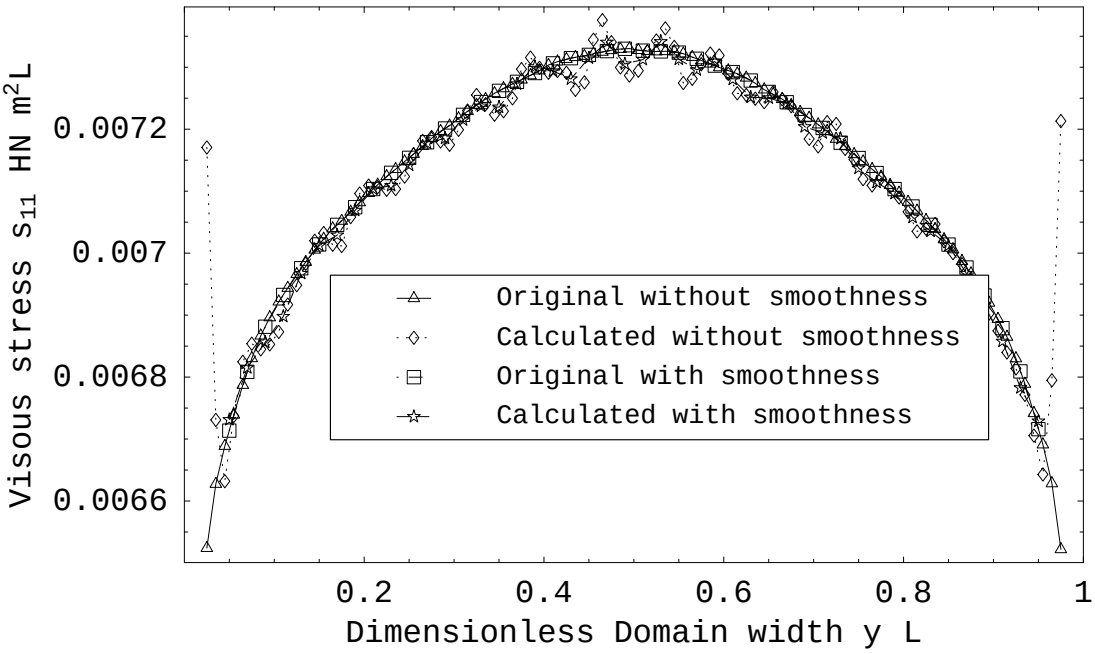

Figure 1: Cross-Channel Couette flow profile of σ_{11} in Case 2 (Kn=0.1, Ma=0.975); original values from the ES-BGK model and calculated values from Eqs. (10), with and without smoothing.

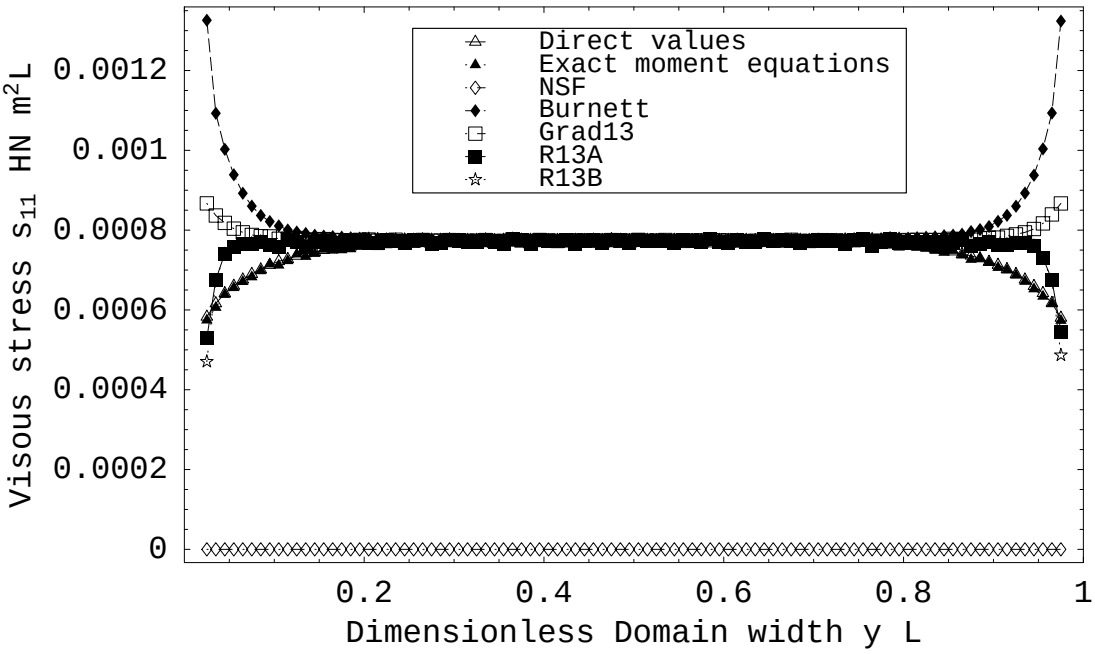

Figure 2: Cross-channel Couette flow profile of σ_{11}; direct values from the ES-BGK model and corresponding calculated values from indicated sets of macroscopic equations; Case 1 (Kn=0.025, Ma=0.975).

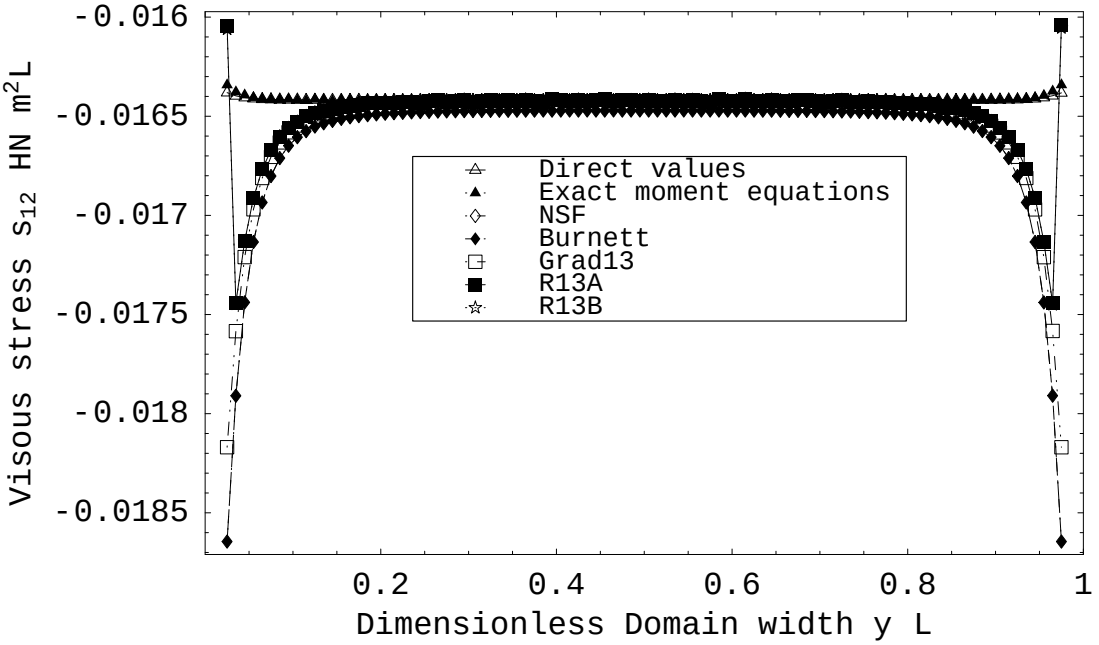

Figure 3: Cross-channel Couette flow profile of σ_{12}; direct values from the ES-BGK model and corresponding calculated values from indicated macroscopic sets of macroscopic equations; Case 1 (Kn=0.025, Ma=0.975).

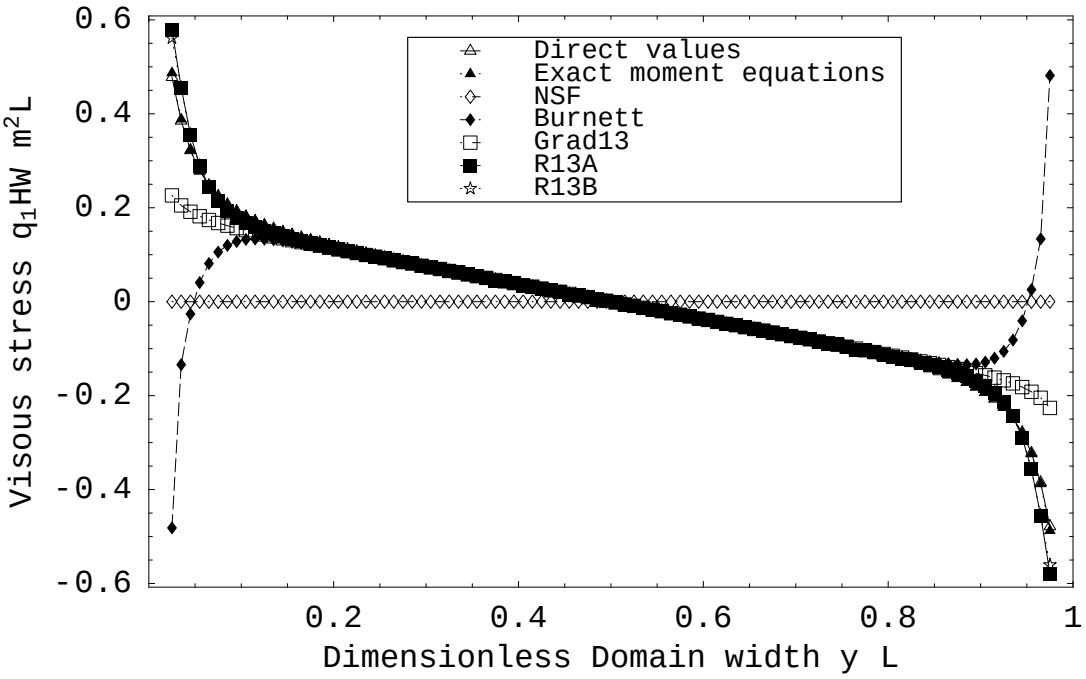

Figure 4: Cross-channel Couette flow profile of q_1; direct values from the ES-BGK model and corresponding calculated values from indicated sets of macroscopic equations; Case 1 (Kn=0.025, Ma=0.975).

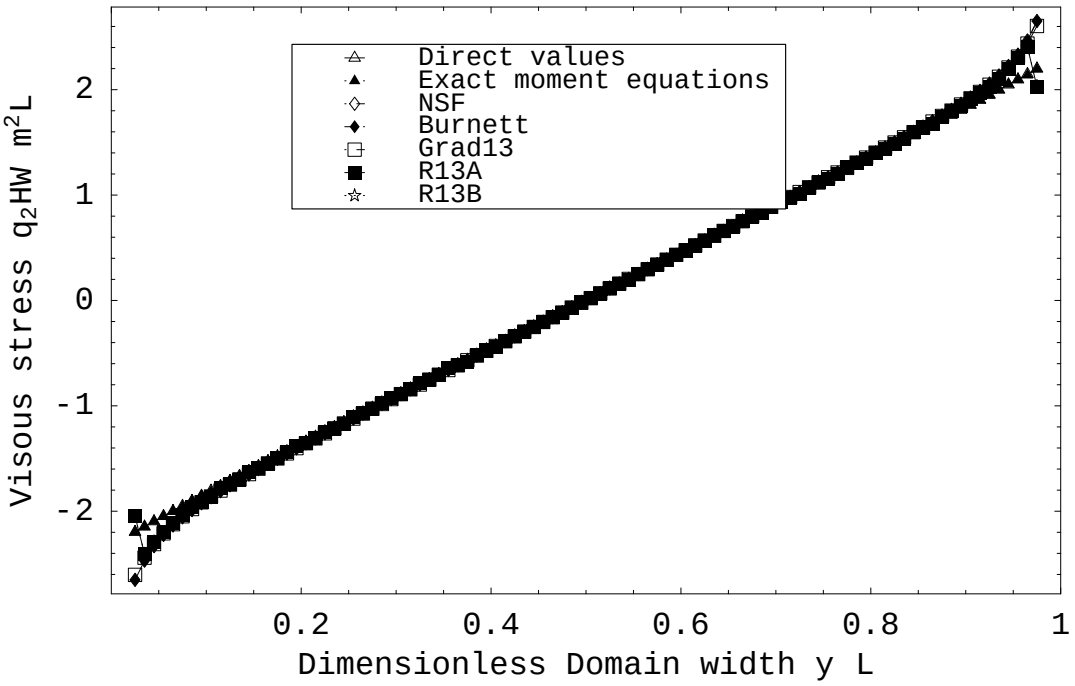

Figure 5: Cross-channel Couette flow profile of q_2; direct values from the ES-BGK model and corresponding calculated values from indicated sets of macroscopic equations; Case 1 (Kn=0.025, Ma=0.975).

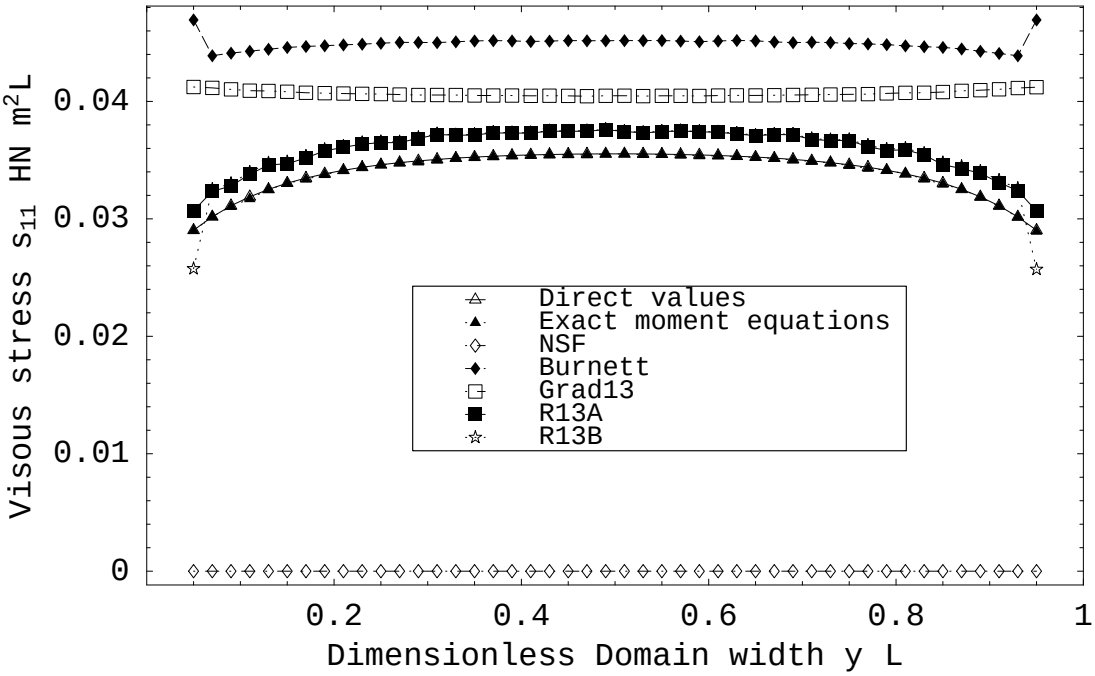

Figure 6: Cross-channel Couette flow profile of σ_{11}; direct values from the ES-BGK model and corresponding calculated values from indicated sets of macroscopic equations; Case 7 (Kn=0.1, Ma=1.950).

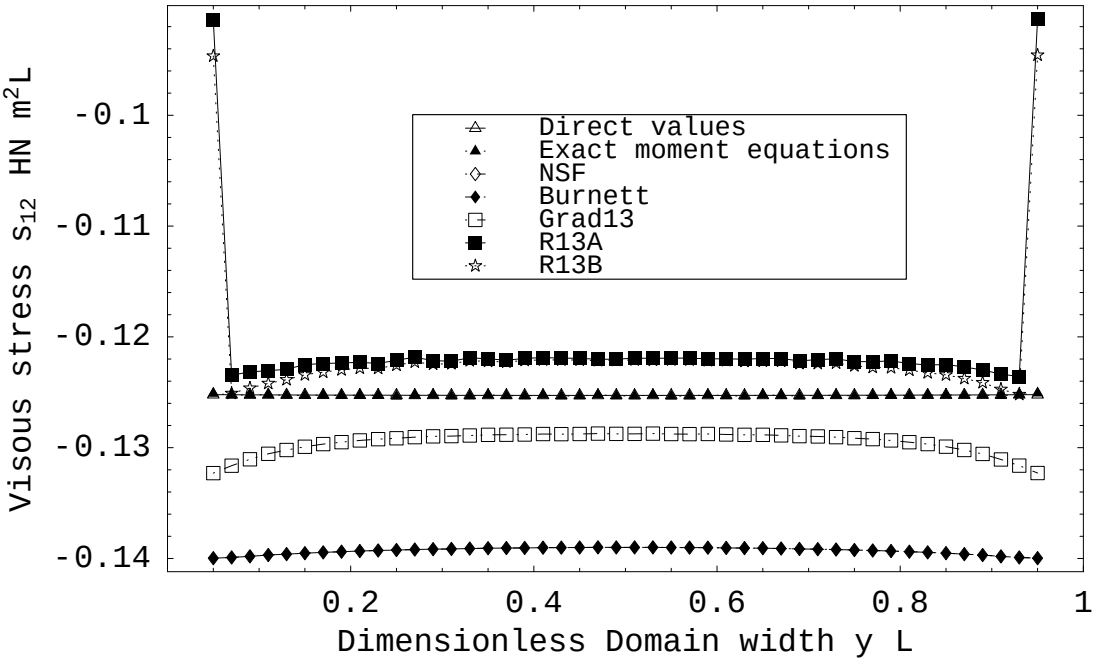

Figure 7: Cross-channel Couette flow profile of σ_{12}; direct values from the ES-BGK model and corresponding calculated values from indicated sets of macroscopic equations; Case 7 (Kn=0.1, Ma=1.950).

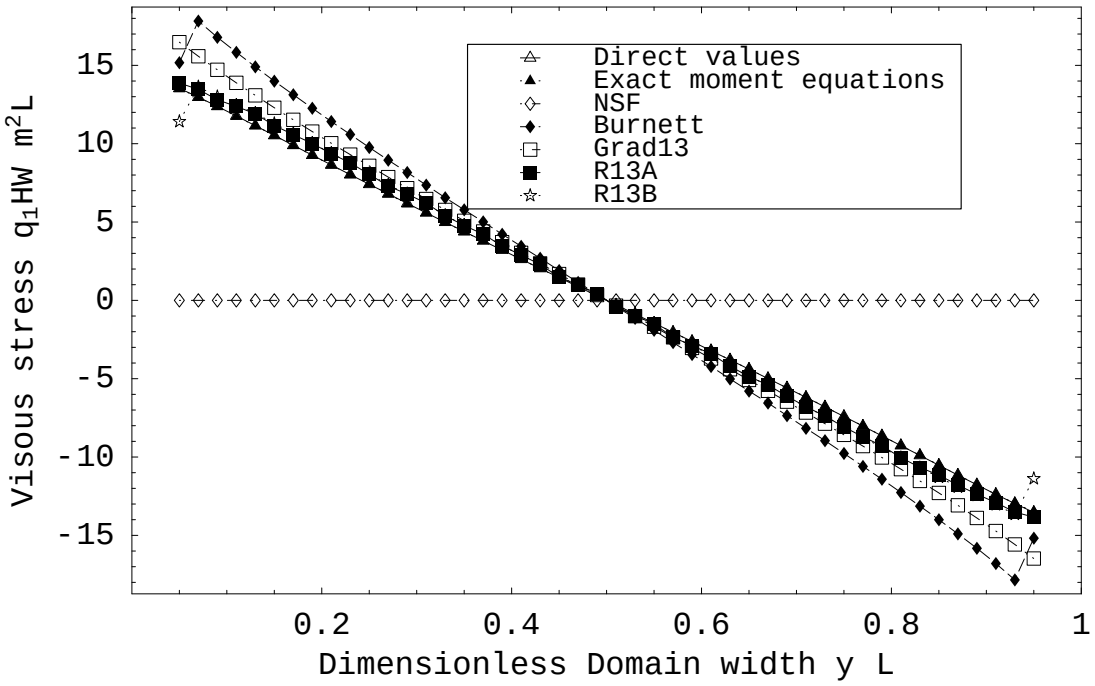

Figure 8: Cross-channel Couette flow profile of q_1; direct values from the ES-BGK model and corresponding calculated values from indicated sets of macroscopic equations; Case 7 (Kn=0.1, Ma=1.950).

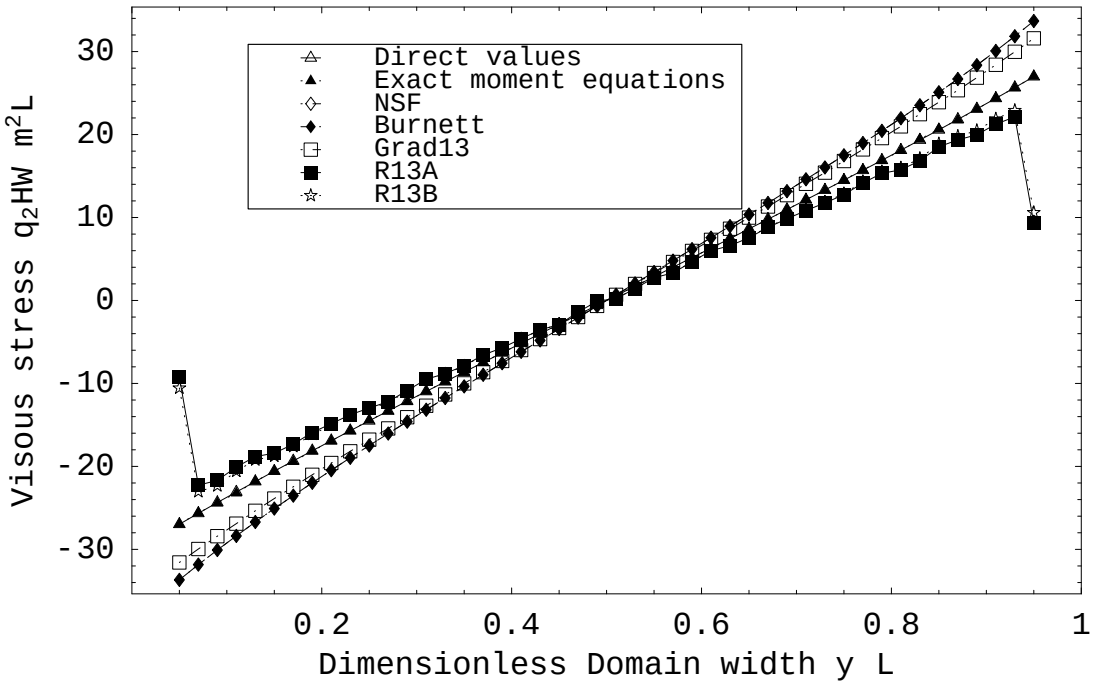

Figure 9: Cross-channel Couette flow profile of q_2; direct values from the ES-BGK model and corresponding calculated values from indicated sets of macroscopic equations; Case 7 (Kn=0.1, Ma=1.950).

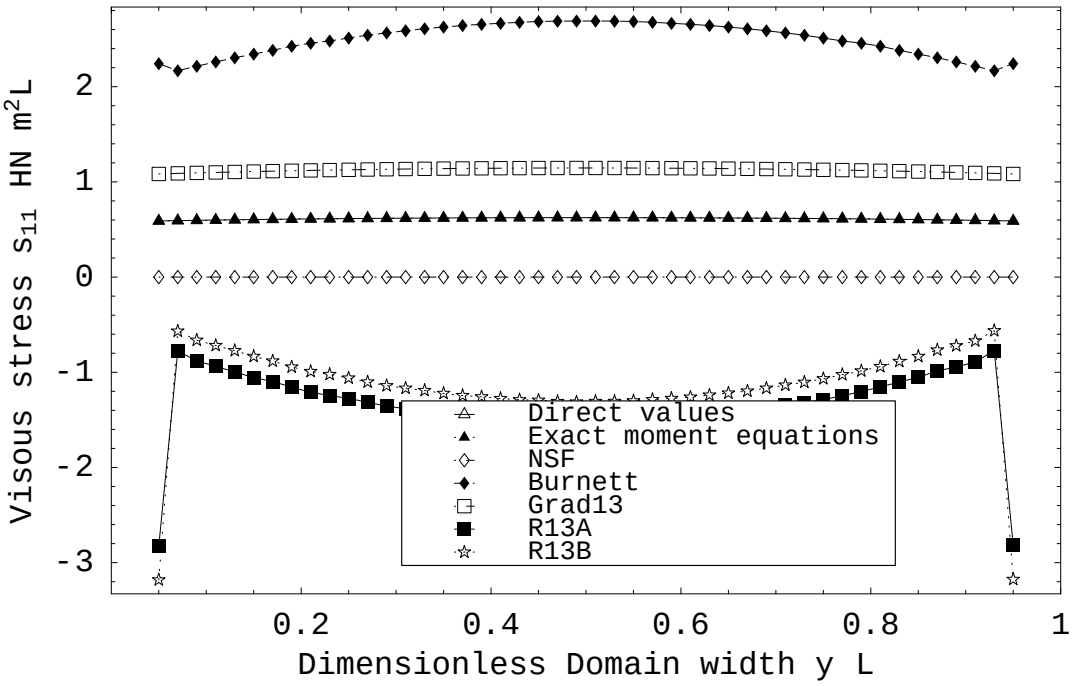

Figure 10: Cross-channel Couette flow profile of σ_{11}; direct values from the ES-BGK model and corresponding calculated values from indicated sets of macroscopic equations; Case 6 (Kn=0.5, Ma=3.251).

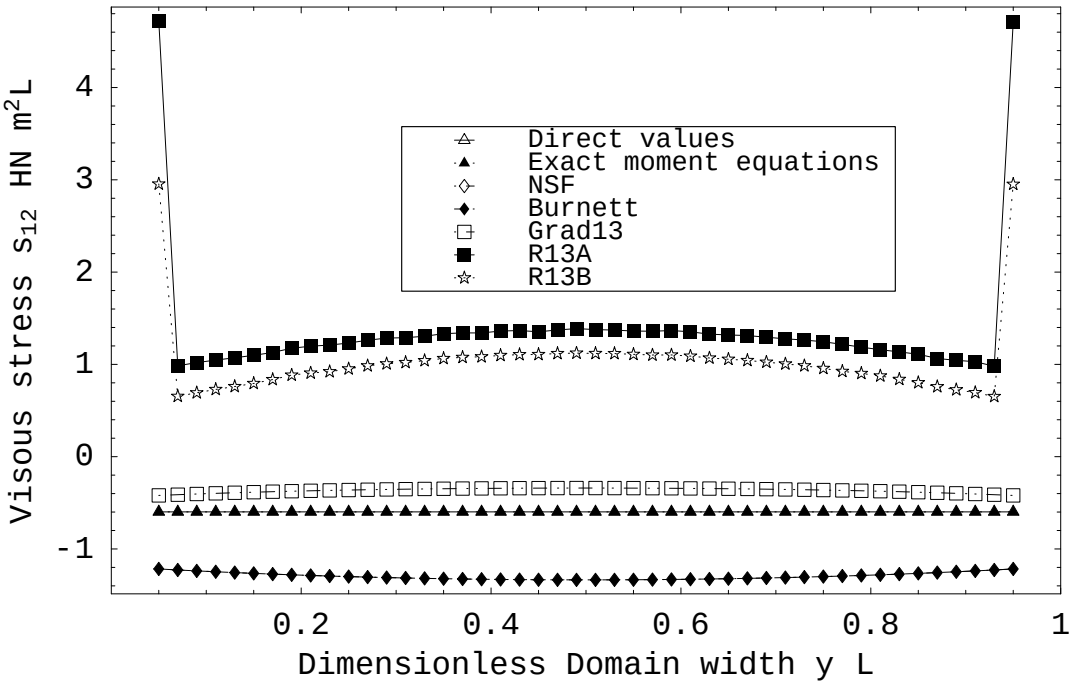

Figure 11: Cross-channel Couette flow profile of σ_{12}; direct values from the ES-BGK model and corresponding calculated values from indicated sets of macroscopic equations; Case 6 (Kn=0.5, Ma=3.251).

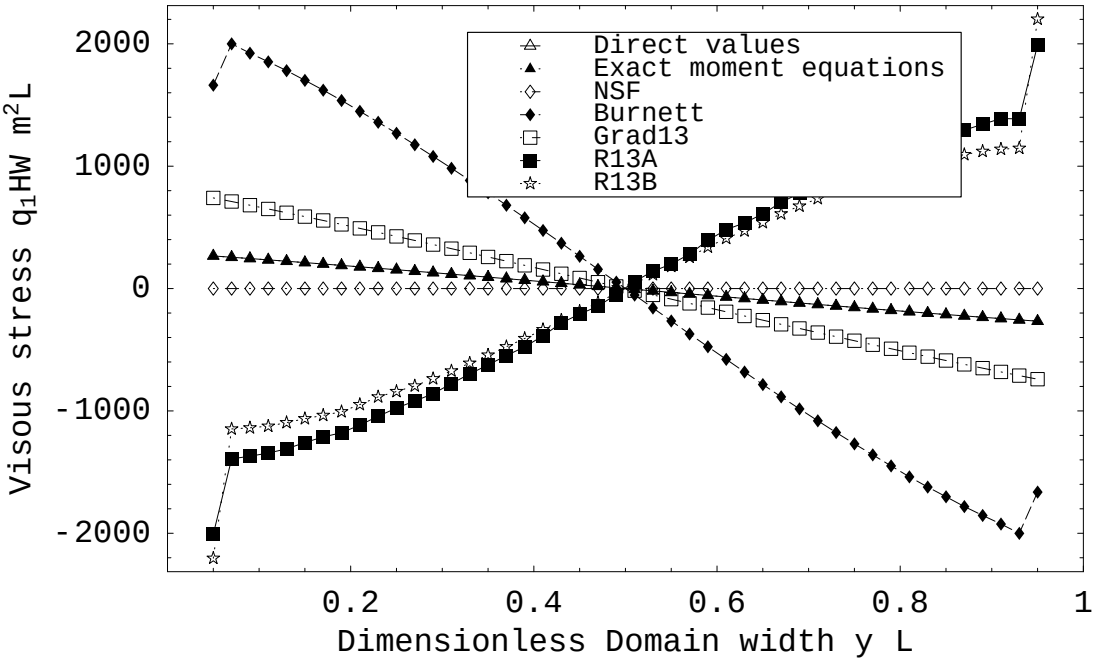

Figure 12: Cross-channel Couette flow profile of q_1; direct values from the ES-BGK model and corresponding calculated values from indicated sets of macroscopic equations; Case 6 (Kn=0.5, Ma=3.251).

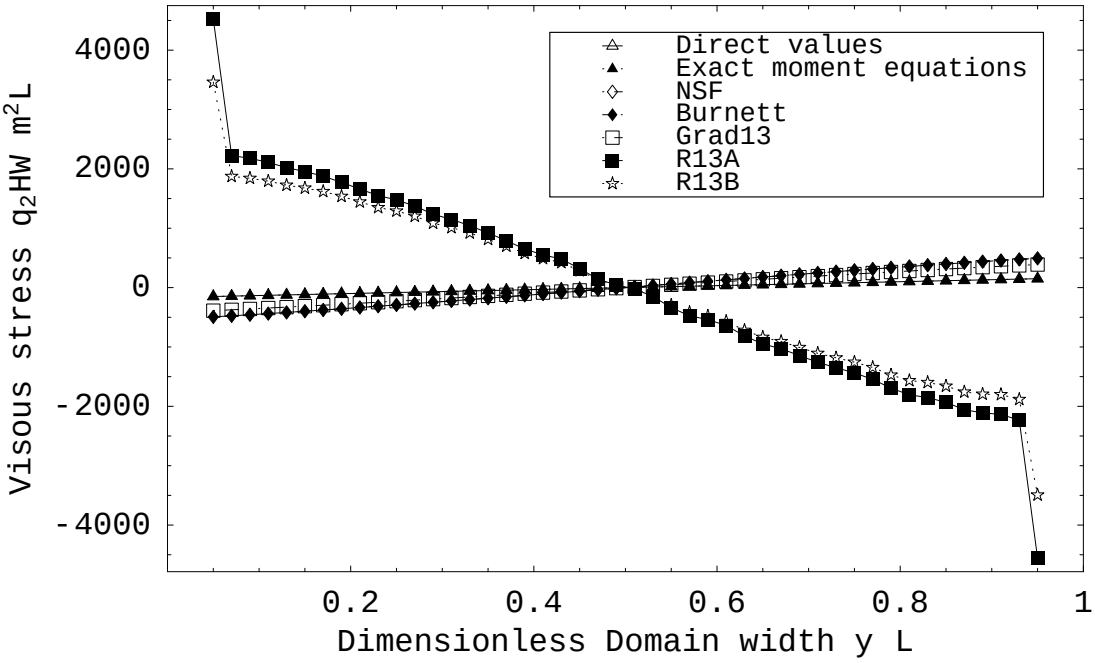

Figure 13: Cross-channel Couette flow profile of q_2; direct values from the ES-BGK model and corresponding calculated values from indicated sets of macroscopic equations; Case 6 (Kn=0.5, Ma=3.251).

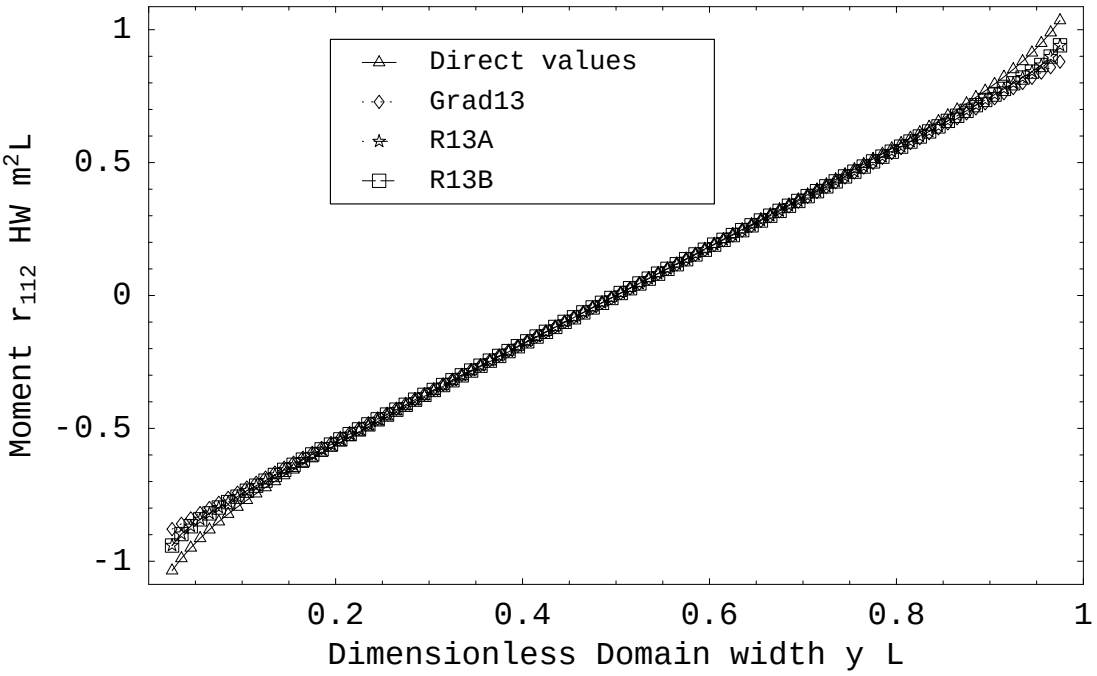

Figure 14: Cross-channel Couette flow profile of $\rho_{<112>}$; direct values from the BGK model and corresponding calculated values from indicated sets of macroscopic equations; Case 1 (Kn=0.025, Ma=0.975).